Large-scale characteristics of stratified wake turbulence at varying Reynolds number

Qi Zhou[1] and Peter J. Diamessis[2]
[1]*Department of Civil Engineering, University of Calgary, Calgary, Alberta, Canada T2N 1N4*
[2]*School of Civil and Environmental Engineering, Cornell University, Ithaca, New York 14853, USA*

(Received 6 June 2019; published 9 August 2019)

We analyze a large-eddy simulation data set of wakes of a towed sphere of diameter D at speed U in a uniformly stratified Boussinesq fluid with buoyancy frequency N and kinematic viscosity ν. These temporally evolving wakes are simulated using a spectral multidomain penalty-method-based incompressible Navier-Stokes solver for $\mathrm{Fr} \equiv 2U/ND \in \{4, 16, 64\}$ and $\mathrm{Re} \equiv UD/\nu \in \{5 \times 10^3, 10^5, 4 \times 10^5\}$, enabling a systematic examination of stratified wakes at three different values of Re sufficiently separated in magnitude. As such, particular attention is paid to the effects of varying Re on the evolution of large-scale characteristics of stratified wake turbulence. We examine the evolution of horizontal and vertical integral length scales (ℓ_h and ℓ_v), horizontal and vertical fluctuation velocities ($\mathcal{U}$ and $\mathcal{W}$), local vertical shear, as well as the resulting dimensionless parameters based on the above quantities. In particular, the vertical turbulent Froude number $\mathrm{Fr}_v^\star \equiv 2\pi\mathcal{U}/N\ell_v$ is found to be of order unity, a signature of the dynamics in the strongly stratified regime where shear instabilities develop between anisotropic flow layers. The horizontal turbulent Reynolds number $\mathrm{Re}_h \equiv \mathcal{U}\ell_h/\nu$ stays approximately constant in time and the horizontal turbulent Froude number $\mathrm{Fr}_h \equiv \mathcal{U}/N\ell_h$ decays in time as $(Nt)^{-1}$, consistent with scaling analysis of freely decaying turbulence. We characterize the transitions between distinct stratified flow regimes and examine the effects of body-based parameters Re and Fr on these transitions. The transition from the weakly to the strongly stratified regime, which is marked by $\mathrm{Fr}_v^\star$ decaying to unity, occurs when $\mathrm{Fr}_h \simeq O(0.01)$. We further show that the initial value of Re_h at which the flow completes the above transition scales as $\mathrm{Re}\,\mathrm{Fr}^{-2/3}$, which provides a way to predict the possibility of accessing the strongly stratified regime for a wake of given Re and Fr. The analysis reported here constitutes an attempt to obtain the predictive capability of stratified wake turbulence in terms of Reynolds number Re, applying select elements of strongly stratified turbulence theory, so far typically utilized for homogeneous turbulence, to a canonical inhomogeneous turbulent free-shear flow.

DOI: 10.1103/PhysRevFluids.4.084802

I. INTRODUCTION

The stratified turbulent wake is a frequently occurring free-shear flow in a number of geophysical and ocean engineering configurations [1]. The wake of a towed sphere is a canonical configuration which has been used to investigate stratified wakes in numerous laboratory (e.g., [2–7]) and numerical (e.g., [8–15]) studies. A stratified turbulent towed-sphere wake is, by design, spatially inhomogeneous in the span-vertical plane and temporally nonstationary in a fixed laboratory reference frame where the flow follows a distinct life cycle. Motivated by the evolution of the centerline mean axial velocity U_0 with respect to the dimensionless time Nt, where $N \equiv \sqrt{(-g/\rho_0)(d\overline{\rho}/dz)}$ is the buoyancy frequency, Spedding [5] divided the wake life cycle into three regimes: (i) a three-dimensional regime for $Nt \in [0, 2]$ where $U_0 \propto t^{-2/3}$, (ii) a nonequilibrium (NEQ) regime for $Nt \in [2, 50]$ where $U_0 \propto t^{-1/4}$, and (iii) a quasi-two-dimensional regime for $Nt \in [50, \infty)$ where

$U_0 \propto t^{-0.76}$. Such a flow regime classification focuses primarily on mean-flow metrics, and it is not clear if a regime classification can be drawn based upon the characteristics of wake turbulence, a question that motivates the present study.

Another significant aspect of Spedding's wake regime classification is, on account of the inherent physical space limitations of the laboratory, the absence of any systematic investigation of the dependence of wake physics on the wake's body-based Reynolds number $\mathrm{Re} \equiv UD/\nu$, where D is the sphere diameter, U is the tow speed, and ν is the kinematic viscosity. Instead, Spedding focused on the effects of $\mathrm{Fr} \equiv 2U/ND$, the body-based Froude number. In contrast to the experiments of Spedding [5], numerical simulations by Diamessis *et al.* [10] at $\mathrm{Re} = 10^5$, a value that is one order of magnitude larger than those obtained in the laboratory, did show qualitative differences in the flow evolution, such as a significant prolongation of the duration of the NEQ regime in higher-Re wakes, due primarily to the emergence of secondary shear instabilities within the large-scale pancake vortices. The effects of varying Re in wakes have also been seen in terms of the internal waves emitted by the wake turbulence [16–18] and the properties of the turbulent-nonturbulent interface [19]. A recent numerical data set [20] brings into play an additional, sufficiently removed data point for Reynolds number at $\mathrm{Re} = 4 \times 10^5$. As such it enables a systematic investigation of the effects of Re on stratified wake turbulence which is presented in this paper, potentially providing insights into the structural and dynamical aspects of this canonical turbulent shear flow at geophysically relevant Re values [1].

Motivated by the scaling argument originally developed by Riley *et al.* [21] and Lilly [22] and later improved by Billant and Chomaz [23], Brethouwer *et al.* [24] proposed a regime classification for stratified flows, based entirely on the characteristics of turbulence (rather than mean flows as in Spedding's wake classification), a theory we briefly review in Sec. II. Presumably due to the ease of numerical implementation, most pioneering computational studies of the various regimes have been conducted in a triply periodic, homogeneous turbulence configuration (e.g., [25–27]), constituting a remarkable series of investigations which laid the foundation for a robust theoretical framework for classifying stratified flows into various flow regimes based upon the relevance of stratification and/or viscosity to the flow dynamics. Stratified wakes, which are representative of a canonical type of localized free-shear flow, provide a unique platform to extend the above theoretical framework which so far has been typically utilized to interpret homogeneous turbulence to an inhomogeneous turbulent flow configuration.

In this paper we investigate the stratified turbulence characteristics in wakes of a towed sphere. Specifically, we focus on the effects of Reynolds number on the characteristics of the large-scale wake turbulence, e.g., how the structure of the coherent pancake vortices can be altered at larger Re, as the energy-containing scales become less affected by viscosity, as well as how the self-selection of vertical integral scale vary with Re and the associated implication for the longevity of turbulence [10]. As will be shown, a distinct strongly stratified regime can exist in wakes for a specific range of body-based wake parameters, and accessing this specific regime can in fact have a significant impact on the evolution of wake turbulence. The main objectives of the paper are thus (i) to examine the flow structure and temporal evolution of the large-scale turbulent characteristics, such as integral lengths and velocity scales, and in particular how they may vary with Re and (ii) to investigate the dynamics and predict the accessibility of the strongly stratified regime in the specific context of stratified turbulent wakes, i.e., in terms of a wake's body-based Reynolds and Froude numbers, i.e., Re and Fr.

To address these questions, we organize the remainder of the paper as follows. In Sec. II we provide a brief review of the relevant scaling arguments and apply it specifically to the context of stratified wake turbulence. In Sec. III the wake configuration under investigation is described and the numerical data set is introduced. In Sec. IV we present qualitative features of the wake turbulence, highlighting the Reynolds-number effects on coherent vortical structures. In Sec. V we describe the time evolution of various characteristics of turbulence, such as length scales, fluctuation velocities, and local vertical shear, followed by Sec. VI, where the relevant dimensionless parameters are discussed, with a focus on the trajectories followed by stratified wake turbulence in an appropriately

defined phase space which sheds light on the flow regime progression. We continue to discuss in Sec. VI the accessibility of the strongly stratified regime, quantifying the implications of varying Re, before we conclude the paper in Sec. VII with a summary of our findings and open questions.

II. SCALING ARGUMENTS FOR STRATIFIED TURBULENCE

A. Strongly stratified regime

Scaling arguments [21–24,28] based on the governing equations of motion have led to the prediction of a distinct flow regime in a strongly stratified fluid. In this regime, which is often referred to as strongly stratified turbulence (SST), the effect of stratification is strong, driving highly anisotropic turbulent structures with a larger horizontal integral scale than the vertical, and viscous effects are weak, allowing for a broad dynamic range between the energy-containing and the viscous or dissipative scales to support turbulence. Such a regime is also referred to as layered anisotropic stratified turbulence (LAST) in recent literature (see, e.g., Sec. II of [29]). An instructive way to identify the potential presence of the SST (or LAST) regime in any given flow is through a diagram plotted on the $(\mathrm{Re}_h, \mathrm{Fr}_h^{-1})$ phase space proposed by Brethouwer *et al.* [24] (see their Fig. 18 and Fig. 1 in the present paper), where Re_h and Fr_h are appropriately defined Reynolds and Froude numbers to describe horizontal turbulent motions:

$$\mathrm{Re}_h \equiv \frac{\mathcal{U}\ell_h}{\nu}, \quad \mathrm{Fr}_h \equiv \frac{\mathcal{U}}{N\ell_h}. \tag{1}$$

Here we interpret $\mathcal{U}$ as the horizontal component of characteristic fluctuation velocity and ℓ_h is a horizontal length-scale representative of the large, energy-containing turbulent motions, e.g., an integral scale. It is then possible to combine Re_h and Fr_h to define a buoyancy Reynolds number

$$\mathcal{R} \equiv \mathrm{Re}_h \mathrm{Fr}_h^2 = \frac{\mathcal{U}^3}{\ell_h}\frac{1}{\nu N^2}. \tag{2}$$

Riley and de Bruyn Kops [26] showed that $\mathcal{R}$ can be used to predict the potential for secondary shear instabilities to emerge in a strongly stratified flow. Brethouwer *et al.* [24] suggested that $\mathcal{R}$ measures the ratio of the vertical advection and diffusion terms in the horizontal momentum equation, if the vertical scale ℓ_v is set by $\mathcal{U}/N$. By examining the vorticity equation, Davidson [30] (see p. 442 therein) showed that $\mathcal{R}$ characterizes the ratio of inertial and viscous forces at the integral scale in a

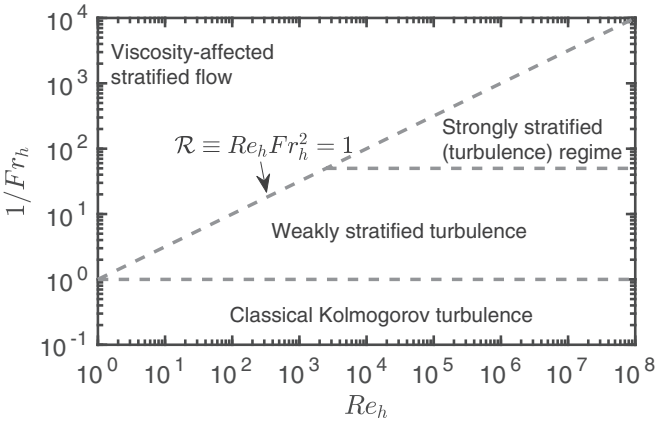

FIG. 1. Parameter space [24] based on turbulent horizontal Reynolds and Froude numbers Re_h and Fr_h, respectively, and the proposed regime classification for stratified flows. Gray dashed lines delineate the proposed transitional boundaries between adjacent regimes.

strongly anisotropic flow and $\mathcal{R} \gg 1$ is required to "ensure that viscous effects are confined to the small scales."

The SST regime occurs in the asymptotic limit where the stratification is strong, i.e.,

$$\mathrm{Fr}_h \ll 1. \tag{3}$$

Furthermore, SST requires that the layered structures at the vertical scale $\mathcal{U}/N$ are not affected by viscosity, i.e.,

$$\mathcal{R} \equiv \mathrm{Re}_h \mathrm{Fr}_h^2 \gg 1. \tag{4}$$

A classical scaling estimate for the dissipation rate ε exists for nonstratified fluids [31], i.e.,

$$\varepsilon \sim \frac{\mathcal{U}^3}{\ell_h}, \tag{5}$$

which has also been applied in the context stratified flows (see, e.g., [25,32]) and is revisited in the remainder of this paper (Appendix B). If Eq. (5) holds, $\mathcal{R}$ scales with the $\varepsilon/\nu N^2$ parameter, which is widely used in the literature (see, e.g., [32]). However, the numerical methodology (see more details in Sec. III and Appendix B) used to generate the data set examined here, lacking an explicit subgrid-scale model, does not allow for direct estimates for ε; quantitative discussion of ε is therefore outside the scope of this paper.

It was hypothesized by Billant and Chomaz [23] that, in the asymptotic limits of $\mathrm{Fr}_h \to 0$, the flow structure may reorganize in a self-similar way under strong buoyancy effects such that the vertical length scale ℓ_v becomes comparable to $\mathcal{U}/N$, i.e.,

$$\ell_v \sim \frac{\mathcal{U}}{N}. \tag{6}$$

In this case ℓ_v is independent of viscosity as the length scale follows the inviscid scaling. Such a self-adjustment of ℓ_v has been observed in numerous simulations of homogeneous turbulence in the SST regime, both forced (e.g., [24]) and unforced (e.g., [33]). Billant and Chomaz [23] showed that the potential and kinetic energies of the flow are of the same order if Eq. (6) holds. Lindborg [25] suggested that a balance of inertia and buoyancy forces would be reached if ℓ_v adjusts to match the scaling in Eq. (6) and thus hypothesized that a forward cascade of energy can exist in a highly anisotropic, strongly stratified flow. Brethouwer *et al.* [24] (see Sec. 2.3 therein) formally defined the SST regime as $\mathcal{R} \gg 1$ and $\mathrm{Fr}_h \ll 1$, a regime for which Eq. (6) is expected to hold such that the vertical advection term in the horizontal momentum equation is of the same order as the horizontal advection terms, and thus the leading dynamics are three dimensional but strongly anisotropic.

On the other hand, when the large-scale motions are strongly affected by viscosity [34], the vertical length scale ℓ_v would adjust in a way such that

$$\frac{\ell_v}{\ell_h} \sim \mathrm{Re}_h^{-1/2}, \tag{7}$$

which is instead a viscous scaling that is reminiscent of a laminar boundary layer (see, e.g., Sec. 10 of [35]). This viscous scaling applies to flows with $\mathcal{R}$ values much smaller than order unity, i.e., the viscosity-affected stratified flow (or viscous) regime (the triangular region in the upper left of the diagram shown in Fig. 1). The two distinct scalings for ℓ_v, i.e., Eqs. (6) and (7), respectively, provide an informative tool to distinguish between the strongly stratified regime and the viscous regime for a given flow. Both scalings will be applied in Sec. V A towards interpreting our stratified wake data.

As scaling arguments only predict that the SST dynamics are operative in the asymptotic limit of $\mathcal{R} \gg 1$, there objectively exists some degree of uncertainty in the threshold value $\mathcal{R}_c$ above which the flow regime can indeed be interpreted as SST. In the context of homogeneous decaying turbulence, Maffioli and Davidson [33] argued that the transition between the SST and the viscous regimes exists for $\mathcal{R}$ of order unity, i.e., $\mathcal{R}_c \sim O(1)$, which is consistent with the

empirical observation of $\mathcal{R}_c \approx 4$ from numerical simulation of the secondary instabilities of the zigzag instability [36]. More recently, de Bruyn Kops and Riley [37] observed that the value of $\mathcal{R}_c \approx 15$ in order to sustain shear instability within the buoyancy-driven shear layers.

In order to stay focused on our primary objective in this paper, i.e., to understand the effect of wake Reynolds number on the regime progression of stratified wake turbulence, and avoid the potential confusion caused by the ambiguity in the threshold $\mathcal{R}_c$ associated with the strictly defined SST terminology, we will instead pursue a more broadly oriented discussion, namely, one considering the regime where $\mathcal{R} > 1$ and $\mathrm{Fr}_h \ll 1$, which will be referred to as the strongly stratified regime. Note that for the $\mathrm{Re} = 4 \times 10^5$ cases examined here, at earlier times, after the establishment of a buoyancy-dominated flow, $\mathcal{R}$ can assume values as high as approximately 40. As such, viscosity does not significantly impact the dynamics of the vertical integral scale, at least until $\mathcal{R}$ drops to values closer to unity in these simulations.

In the context of the broader discussion proposed above, the strongly stratified regime is interpreted as a dynamical state in which the stratification effects are strong as experienced by the horizontal integral scale ($\mathrm{Fr}_h \ll 1$) and the viscous effects have started to influence but not yet to dominate the dynamics of the anisotropic flow layers ($\mathcal{R} > 1$); the latter requirement is in contrast to the strictly defined SST which requires $\mathcal{R} \gg 1$, i.e., viscous effects are completely negligible at the vertical scale $\mathcal{U}/N$ characteristic of the layered structure. As indicated above, the $\mathrm{Re} = 4 \times 10^5$ wakes considered here may potentially reside in the SST regime, a question which nevertheless is outside the scope of this paper. Additionally, as will be shown, some vigorous turbulence can still exist in stratified wakes when $\mathcal{R} \sim O(1)$, albeit in a spatially intermittent fashion, even though aforementioned scaling arguments suggest that viscosity may have some leading-order effects on the dynamics at the vertical integral scale.

B. Regime transitions in stratified turbulence

As will be shown, as the wake evolves in time, the stratified flow within the wake may or may not decay through the strongly stratified regime, depending on the externally specified body-based Reynolds and Froude numbers of the wake. To elucidate the flow regime progression in different wakes and examine the Reynolds-number dependence, we are to first define these regime transitions quantitatively, i.e., the entrance into the strongly stratified regime, as well as the exit from it, both in the specific context of stratified wakes. In the remainder of the paper, a superscript † will be used for quantities associated with the entrance to strongly stratified regime and ‡ for the exit from this regime.

(i) Transition †. As first proposed in Ref. [23], the perhaps most significant feature of a flow within the strongly stratified regime is the self-selection of a vertical length scale according to Eq. (6), i.e., when the vertical turbulent Froude number

$$\mathrm{Fr}_v \equiv \frac{\mathcal{U}}{N\ell_v} \tag{8}$$

becomes order unity (see, e.g., Sec. 14.2 of Ref. [30]). The simulations of decaying homogeneous stratified turbulence by Maffioli and Davidson [33], for instance, observe that the value of Fr_v asymptotes at approximately 0.34–0.37, and it is argued that $\mathrm{Fr}_v \sim O(1)$ can be interpreted as a balance between baroclinic generation and advection terms in the budget for horizontal vorticity (analogous to ω_y in the context of stratified wakes visualized in Fig. 5). The exact value of Fr_v characteristic of the strongly stratified regime, however, should be dependent on the specific definition of quantities such as ℓ_v and $\mathcal{U}$. For example, in a flow where mean velocity components are present, whether to include the mean flows in the calculation of $\mathcal{U}$ could obviously affect the numerical values of Fr_v (and, for that matter, Re_h or $\mathcal{R}$).

An alternative interpretation of the vertical Froude number can be made [21,38,39] in terms of competing timescales, i.e., the advective timescale of horizontal vortices $\ell_h/\mathcal{U}$ and an internal gravity wave timescale (i.e., period) $\ell_h/N^\star\ell_v$ for a flow structure of characteristic horizontal and

vertical length scales ℓ_h and ℓ_v, respectively. The latter timescale $\ell_h/N^\star\ell_v$ can be deduced from the linear dispersion relation of internal waves, and it is perhaps more appropriate to use the cyclical frequency $N^* \equiv N/2\pi$ instead of the radial frequency N in defining such a wave period. Motivated by the above timescale arguments, we will define the entrance to the strongly stratified regime as the time at which the cyclical vertical Froude number $\mathrm{Fr}_v^\star \equiv \mathcal{U}/N^\star\ell_v = 2\pi\mathrm{Fr}_v$ assumes the value of unity, i.e.,

$$\mathrm{Fr}_v^{\star,\dagger} \equiv 1 = 2\pi\mathrm{Fr}_v^\dagger. \tag{9}$$

At this particular time, the advective timescale equals the internal wave period, implying a strong influence of buoyancy on the large-scale motions. Similar definitions of turbulent Froude number which include a factor 2π can be found in several studies of homogeneous stratified turbulence [21,26,37].

(ii) Transition ‡. When no form of forcing is applied to reenergize the flow, as is the case for stratified wakes, turbulence will inevitably decay due to viscous dissipation, unlike forced simulations where the turbulent kinetic energy is maintained at an approximately constant level (see, e.g., [40–42]). As is discussed in Sec. II B, we will define the exit time from the strongly stratified regime to be when the buoyancy Reynolds number $\mathcal{R} \equiv \mathrm{Re}_h\mathrm{Fr}_h^2$ assumes the value of unity, i.e.,

$$\mathcal{R}^\ddagger \equiv 1. \tag{10}$$

At this particular time, viscous effects start to have significant impact on the layered structure, marking an end to the strongly stratified regime as there is insufficient dynamic range to support any sufficiently energetic turbulence over the entire volume of the flow. Nevertheless, as shown in Fig. 4(c) and discussed in Sec. IV, the time when $\mathcal{R} \approx 1$ in a stratified wake flow does not signify the time when all turbulent motions across the entire wake core are completely controlled by viscosity, as spatially intermittent turbulent events might still be present within the wake. The latter transition into a viscously controlled flow, with full suppression of any turbulent fine structure, occurs later in the wake evolution when $(\ell_v/\ell_h)\mathrm{Re}_h^{1/2} \approx 1$, as indicated by Eq. (7), in the limit of $\mathcal{R} \ll 1$.

In the remainder of the paper, the above definitions will be used to approximate the points at which the regime transitions occur. Due to the nature of scaling arguments upon which these regimes are defined, the cutoff values for the regime transitions given in Eqs. (9) and (10) are chosen, inevitably, on a somewhat *ad hoc* basis. Readers are thus advised to focus on how these transitions vary with the control parameters (Re and Fr) across different wakes rather than on the exact points at which the transitions occur; the latter delineation may simply depend on the specific definitions of these transitions.

III. SUMMARY OF NUMERICAL SIMULATIONS

In this paper we investigate stably stratified towed-sphere wakes (Fig. 2) which are characterized by the body-based Reynolds number $\mathrm{Re} \equiv UD/\nu$ and Froude number $\mathrm{Fr} \equiv 2U/ND$. The angular buoyancy frequency N is expressed in terms of radians per unit time, a convention that is followed in this paper. The Prandtl number considered in our simulations is equal to unity, i.e., the molecular diffusivity of the active scalar equals the kinematic viscosity.

The numerical data set analyzed in this paper is generated through implicit large-eddy simulations (ILESs) using an incompressible Navier-Stokes solver based on a spectral multidomain penalty method developed by Diamessis *et al.* [9] invoking the Boussinesq approximation. This solver employs Fourier discretizations in both horizontal directions x (streamwise) and y (spanwise) and a Legendre-polynomial-based spectral multidomain scheme in the vertical direction z. Spectral filtering and a penalty scheme ensure the numerical stability of the simulations without resolving the full spectrum of turbulent motions. Details on the configuration of the numerical scheme can be found in Ref. [10]. These towed-sphere wake simulations do not explicitly compute the flow around the sphere. Instead, the temporally evolving wakes are initialized using a nontrivial scheme of two

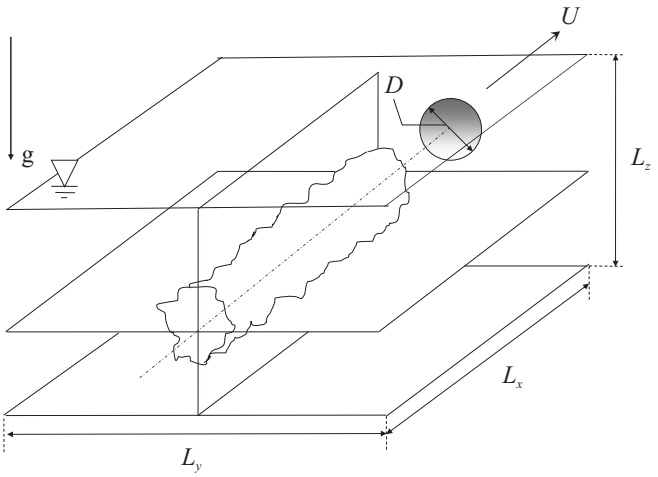

FIG. 2. Computational domain for implicit large-eddy simulation of a temporally evolving, stratified towed-sphere wake [9,10,16,18,19]. The centerline of the wake is at $(y, z) = (0, 0)$. The effect of the towed sphere is not computed explicitly by the Navier-Stokes solver but rather introduced as a complex two-stage turbulent wake initialization procedure [10]. The sphere is assumed to be towed along the x axis, which is the only statistically homogeneous direction in these simulations. The dimensions of the computational domain in this schematic are not drawn to scale.

stages of auxiliary simulations (see [10] for a full discussion) to obtain a self-similar approximation of the near-wake flow field at a downstream distance of $2D$ from the sphere. Readers can also find a summary of the initialization scheme in Sec. 2.3 of Ref. [18].

Full information regarding the wake data set is documented in detail by Zhou [20]. Three values of Re are considered here: 5×10^3, 10^5, and 4×10^5. For the two lower Re values, simulations are conducted for Fr = 4, 16, and 64; these simulations have been reported by Zhou and Diamessis [18] with a focus on the far-field evolution of turbulence-generated internal gravity waves. For the largest Re considered by Zhou [20], i.e., $\mathrm{Re} = 4 \times 10^5$, the same set of Fr values was initially used to carry out the simulations. It was unfortunately discovered later that an input error in configuring the wave-absorbing sponge layer was committed at the initialization stage of the simulation for $(\mathrm{Re}, \mathrm{Fr}) = (4 \times 10^5, 64)$, a simulation that is thus excluded from the discussion in this paper. Specifications of the remaining eight simulations are summarized in Table I. Hereinafter, each simulation will be labeled as RaFb, where $a = \mathrm{Re}/10^3$ and $b = \mathrm{Fr}$.

As tabulated in Table I, which summarizes the ILESs performed, the R5 and R100 simulations are performed in wider and taller domains than the R400 simulations to allow for an investigation of wake-emitted internal waves in the wake's far field [18]. The domains for R400 simulations are made narrower (in y) and shorter (in z) to curb computational cost, as our focus is primarily on the localized wake turbulence near the wake centerline at $(y, z) = (0, 0)$ (Fig. 2). To facilitate a direct comparison in terms of the grid resolution across Reynolds numbers, we report in Table I the number of vertical grid points ($\hat{N}_z$) allocated, in each simulation, within an interval of $z/D \in [-6, 6]$, which corresponds to the full vertical extent of the computational domain for the R400 simulations. The L_y values reported are the initial domain widths in the spanwise direction at the beginning of each wake simulation. In response to the growing wake width in time, the y direction is subject to regridding to provide adequate domain width for the wake to evolve freely without significant interference with the wake's periodic images (see implementation details in [10]). The vertical subdomain distributions (Fig. 3) are adjusted according to Re to ensure adequate resolution of relevant length scales in the vertical direction. Specifically, the vertical resolution of the R100 and R400 simulations is comparable to the direct numerical simulations (DNSs) reported by Watanabe *et al.* [19], who

TABLE I. Summary of implicit large-eddy simulations at various wake Reynolds and Froude numbers. Here L_x, L_y, and L_z are the domain dimensions and $N_x \times N_y \times \hat{N}_z$ is the number of grid points; $\hat{N}_z$ corresponds to the number of grid points allocated to the interval $z/D \in [-6, 6]$, which corresponds to the full vertical extent of the computational domain for the R400 simulations.

Index	Re	Fr	$L_x \times L_y \times L_z$	$N_x \times N_y \times \hat{N}_z$
R5F4	5×10^3	4	$\frac{80}{3}D \times 40D \times 15D$	$256 \times 384 \times 248$
R5F16	5×10^3	16	$\frac{80}{3}D \times 40D \times 15D$	$256 \times 384 \times 248$
R5F64	5×10^3	64	$\frac{80}{3}D \times \frac{160}{3}D \times 17D$	$256 \times 512 \times 248$
R100F4	10^5	4	$\frac{80}{3}D \times 40D \times 15D$	$512 \times 768 \times 695$
R100F16	10^5	16	$\frac{80}{3}D \times 40D \times 15D$	$512 \times 768 \times 695$
R100F64	10^5	64	$\frac{80}{3}D \times \frac{160}{3}D \times 17D$	$512 \times 1024 \times 695$
R400F4	4×10^5	4	$\frac{80}{3}D \times \frac{40}{3}D \times 12D$	$1024 \times 512 \times 1106$
R400F16	4×10^5	16	$\frac{80}{3}D \times \frac{40}{3}D \times 12D$	$1024 \times 512 \times 1106$

obtained fully resolved flow fields by initializing their simulations by select flow fields taken from the ILES data set reported here; according to the same DNS data set [19], the horizontal grid spacing in our ILES is no more than 20 times the Kolmogorov scale. Readers are referred to Appendix A for further details regarding a detailed description of the numerical configuration with regard to the adequacy of resolution as the Reynolds number is varied in these simulations. Herein a stratified towed-sphere wake is investigated numerically at a Re value up to 4×10^5 to examine the wake's full life cycle. The computational costs (in terms of CPU hours) associated with these simulations are $O(10^3)$ for each R5 simulation, $O(10^4$–$10^5)$ for each R100 simulation, approximately 2.0×10^6 for R400F4, and 5.0×10^6 for R400F16. Due to the considerably large computational costs, simulation at even higher Re is presently beyond our capacity.

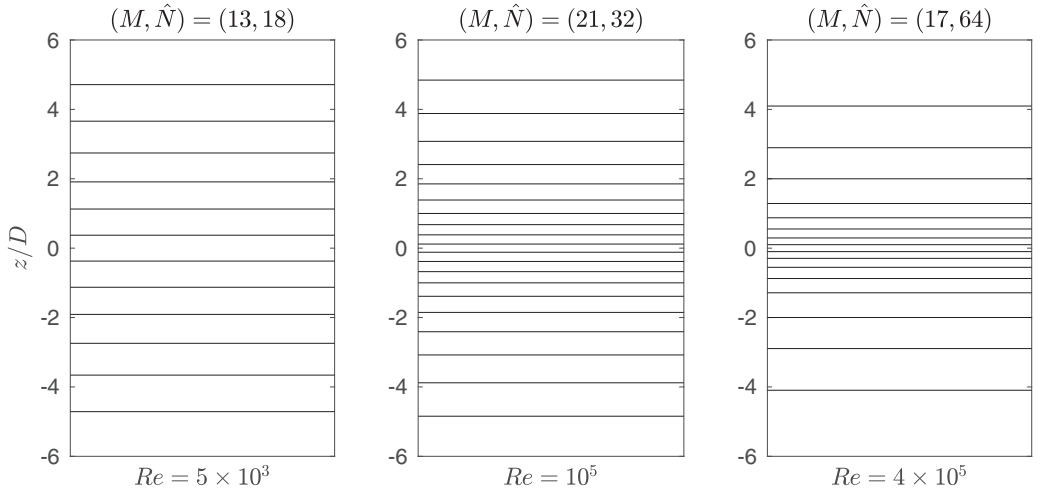

FIG. 3. Subdomain distributions for all three Reynolds numbers on the $z/D \in [-6, 6]$ interval. The black horizontal lines delineate subdomain interfaces with the local Gauss-Lobatto-Legendre grid points omitted for clarity. The total number of grid points for $z/D \in [-6, 6]$ is given by $\hat{N}_z = M(\hat{N} + 1) + 1$, i.e., as reported in Table I. Here M is the number of subdomains, and $\hat{N}$ is the order of polynomial approximation.

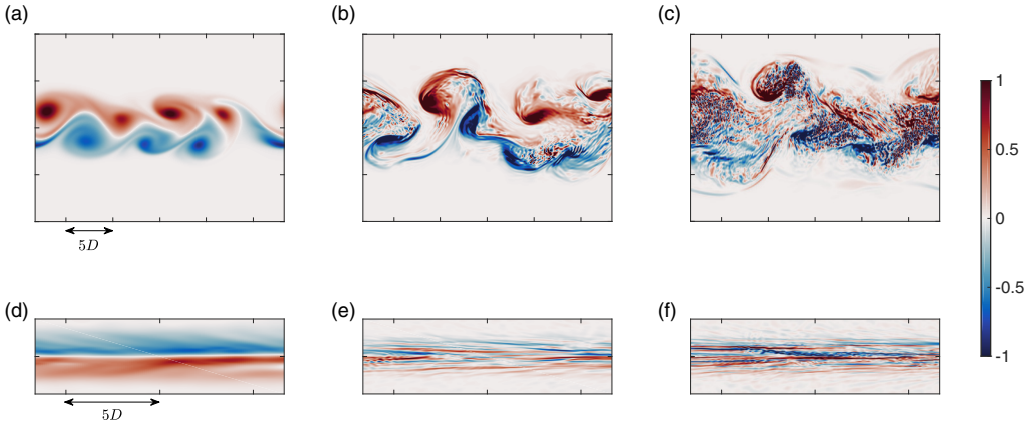

FIG. 4. Colormaps of (a)–(c) vertical vorticity $\omega_z(x, y)$ fields at $Nt = 120$ sampled at the Oxy horizontal midplane ($z = 0$) for simulations R5F4, R100F4, and R400F4, respectively (from left to right) and (d)–(f) spanwise vorticity $\omega_y(x, z)$ fields for the same instances sampled at the Oxz vertical midplane ($y = 0$). The sphere travels from left to right. The length of the visualization window is (a)–(c) $\frac{80}{3}D$ in x and $20D$ and (d)–(f) $\frac{40}{3}D$ in x and $4D$ in z. The colorbar limits are (a)–(c) $\pm 0.09(U/D)$, (d) $\pm 0.15(U/D)$, and (e) and (f) $\pm 0.6(U/D)$.

IV. BASIC PHENOMENOLOGY

Initial appreciation of the qualitative effects of varying Re on the characteristics of wake turbulence can be obtained by examining the vortical structures shown in Fig. 4 at the same time ($Nt = 120$) for the same Froude number (Fr = 4) but varying Reynolds number from $\mathrm{Re} = 5 \times 10^3$ to 4×10^5. At this time instant shown, turbulence in all three cases has self-adjusted under the effects of buoyancy into a highly anisotropic state, i.e., the horizontal turbulence length scale ℓ_h is much larger than its vertical counterpart ℓ_v (quantitative information on these length scales is reported in Sec. V C). As can be seen from the vertical vorticity ω_z field shown in Fig. 4(a), the R5F4 wake has progressed well into the quasi-two-dimensional regime [5], where the highly coherent, quasihorizontal pancake vortices dominate the flow and presumably grow in size through vortex pairing and viscous diffusion [6]. The vertical transect of ω_y for R5F4 in Fig. 4(d) shows rather diffuse layers of spanwise vorticity ω_y (dominated by the vertical gradient of u velocity) without visible disturbances.

In contrast, for the two higher-Re wakes [Figs. 4(e) and 4(f)], the thickness of the shear layers is markedly reduced and the magnitude of the vertical shear is enhanced [note that the colorbar limits are quadrupled in Figs. 4(e) and 4(f) compared to those in Fig. 4(a) to avoid oversaturation of colors]. What appear to be local shear instabilities within the vorticity layers are clearly visible in Figs. 4(e) and 4(f), in the form of localized patches of disturbances strongly reminiscent of the observations by Riley and de Bruyn Kops [26] and Diamessis *et al.* [10]. These secondary disturbances within shear layers appear to be more space filling for the R400F4 case [Fig. 4(f)] than for R100F4 [Fig. 4(e)]. Consistent with the observations drawn from the ω_y field, the degree of coherence and smoothness exhibited by the ω_z field [Figs. 4(a)–4(c)] is significantly reduced as Re increases, to a degree such that only a hint of the coherent pancake vortices are discernible in the R400F4 wake [Fig. 4(c)]. Instead, the vortical structures are dominated by small-scale turbulent patches that are presumably driven by the local shear instabilities between the highly anisotropic vorticity layers [Fig. 4(f)]. Note that these intermittently distributed turbulent patches occur at a time when $\mathcal{R} \sim O(1)$, as discussed in the next section.

Figure 5 shows representative vertical transects of spanwise vorticity ω_y at Fr = 16 for all three Re values, highlighting the evolution of such structures in time. Similar to the visualizations for

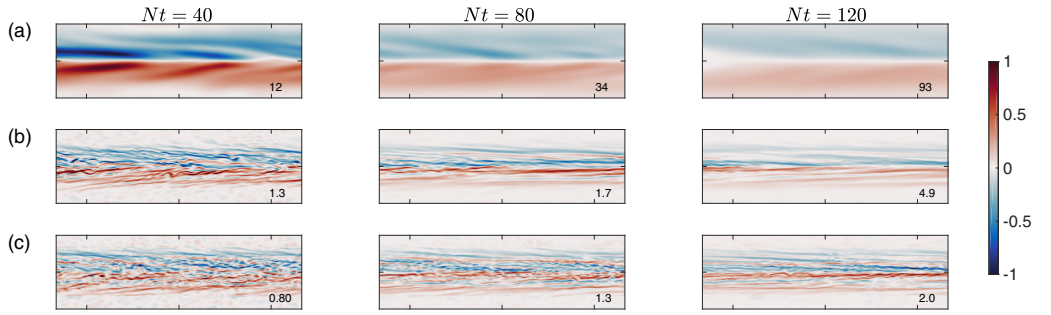

FIG. 5. Colormaps of spanwise vorticity $\omega_y(x, z)$ fields at $Nt = 40$, 80, and 120, respectively (from left to right) sampled at the Oxz vertical midplane ($y = 0$) for simulations (a) R5F16, (b) R100F16, and (c) R400F16, respectively. The length of the visualization window is $\frac{40}{3}D$ in x and $4D$ in z. The colorbar limits are (a) $\pm 0.09(U/D)$ and (b) and (c) $\pm 0.36(U/D)$. The median value of the local gradient Richardson number $\mathrm{Ri}_{g,\mathrm{loc}}$ at each time instance is marked in the bottom right corner of each panel.

$\mathrm{Fr} = 4$ (see Fig. 4), the vorticity layers in the R5F16 wake [Fig. 5(a)] are free from secondary disturbances and the magnitude of shear is reduced significantly with time (presumably due to viscous diffusion), as can be seen from the fading of color contrast with time (same colorbar limits are used for all times shown in the same panel). The R100F16 and R400F16 wakes exhibit larger values of local shear than R5F16 [again, the colorbar limits in Figs. 5(b) and 5(c) are quadrupled with respect to that in Fig. 5(a)]. The magnitude of spanwise vorticity has been reduced by $Nt = 120$ for all Re values, but not as significantly for R100F16 and R400F16 as for R5F16. The secondary disturbances become increasingly sparse for later times, a trend that is accompanied by increasing values of local gradient Richardson number $\mathrm{Ri}_{g,\mathrm{loc}}$ (see the quantitative discussion in Sec. V). Here $\mathrm{Ri}_{g,\mathrm{loc}}$ can be interpreted as an indicator of the tendency for shear instabilities to form within the buoyancy-driven vorticity layers (e.g., as used by Riley and de Bruyn Kops [26]). The secondary disturbances are still visible in the R400F16 wake at a time as late as $Nt = 120$, i.e., approximately 20 buoyancy periods since the passage of the sphere, whereas the disturbances have almost completely vanished in the R100F16 wake at the same time. (Readers are referred to Sec. 7.2 of Ref. [20] where more details on the evolution of the vortical structures are reported).

V. STRATIFIED TURBULENCE CHARACTERISTICS

A. Turbulent integral length scales

We first discuss the time evolution of the turbulent length scales since they follow distinct scalings as the wake turbulence progresses through various flow regimes (see the review in Sec. II). Figure 6 shows the time series of the integral length scales in the vertical and horizontal directions, i.e., ℓ_v and ℓ_h, respectively, both normalized by the sphere diameter D. These length scales can be interpreted as an integral scale characteristic of the energy-containing motions, and the estimation procedure for these length scales from the turbulence spectra is described in Appendix C. The lengths ℓ_v and ℓ_h are not to be confused with the wake's half-height and half-width, computed through the mean flow profiles and denoted by L_V and L_H, respectively (see Appendix C), which are not the focus of the present discussion.

In examining Fig. 6, it is first to note that the vertical length scale ℓ_v is typically much smaller than the horizontal length scale ℓ_h, corresponding to turbulent structures of very small aspect ratio ℓ_v/ℓ_h. The vertical length scale ℓ_v plotted in Figs. 6(a) and 6(c) varies very weakly with time, a key observation for our further analysis. The wakes of larger Fr values typically correspond to larger values of ℓ_v/D. As the wake's Reynolds number Re is increased from 5×10^3 (R5) to 10^5 (R100), the ℓ_v/D values decrease significantly [as can be seen by comparing Figs. 6(a) and 6(c)], whereas

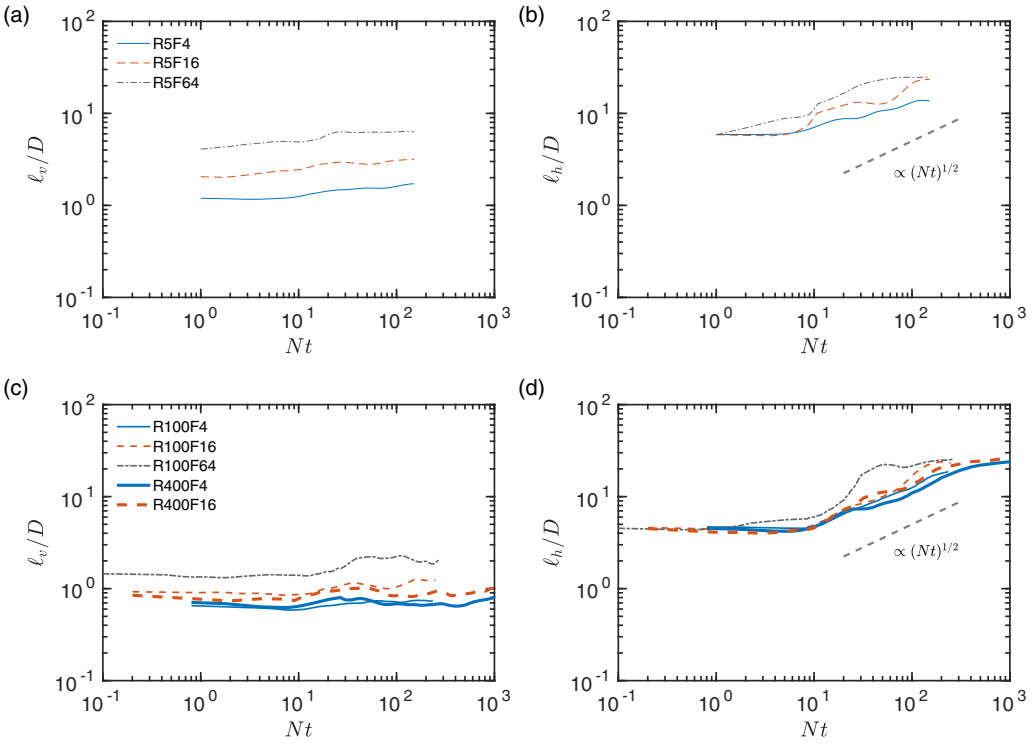

FIG. 6. Time evolution of (a) and (c) vertical turbulence length scale ℓ_v and (b) and (d) horizontal turbulence length scale ℓ_h, both normalized by the sphere diameter D. Results are shown for (a) and (b) $\mathrm{Re} = 5 \times 10^3$ (R5) and (c) and (d) $\mathrm{Re} = 10^5$ and 4×10^5 (R100 and R400, respectively). The line legends are shown in (a) and (c). The line types and colors distinguish various Fr values, and increasing thickness of lines corresponds to a larger value of Re, a scheme that is followed throughout this paper.

when Re is increased from 10^5 (R100) to 4×10^5 (R400), the reduction in ℓ_v is not as significant [Fig. 6(c)]. As will be shown, the R100 and R400 wakes do access the strongly stratified regime after residing in the weakly stratified turbulence regime (Fig. 1), whereas the R5 wakes progresses from weakly stratified turbulence regime directly into the viscous regime.

Figure 6(d) shows that the ℓ_h/D values are relatively insensitive to Re or Fr for the R100 and R400 wakes, in contrast to Fig. 6(b) where some dependence on Fr is observed for the R5 wakes. As shown in Fig. 6(d), the ℓ_h/D values for the R100 and R400 wakes, remain constant at early times, potentially in response to the wake initialization procedure. Similar early-time behavior of horizontal length scales, i.e., $\ell_h \propto t^0$, is observed in DNS of decaying stratified homogeneous turbulence and could be interpreted as an initialization-linked transient [43]. The ℓ_h/D values for the R100 and R400 wakes start to grow after $Nt \simeq 10$. For these wakes [Fig. 6(d)], the power-law growth rate is close to the theoretical prediction of $t^{0.5}$, i.e., Eq. (B7), which is detailed in Appendix B. The curve corresponding to R100F64 notably deviates from the prediction. This is perhaps due to the fact that the R100F64 wake enters the viscous regime at an early time, i.e., $Nt \lesssim 15$, and the length scales are influenced by vortex merging events (similar to those in the later-times of R5 wakes; see also [5]) which are not the focus of this study. Perhaps for the same reason, the R5 wakes [Fig. 6(b)], for which the viscous dynamics dominate after $Nt \gtrsim 10$ [see Fig. 7(b)], do not appear to match the $t^{0.5}$ growth very closely.

Figure 7 examines the competing buoyancy and viscous scalings of the vertical length scale, i.e., Eqs. (6) and (7) respectively. In Figs. 7(a) and 7(c), the inverse cyclical vertical Froude number,

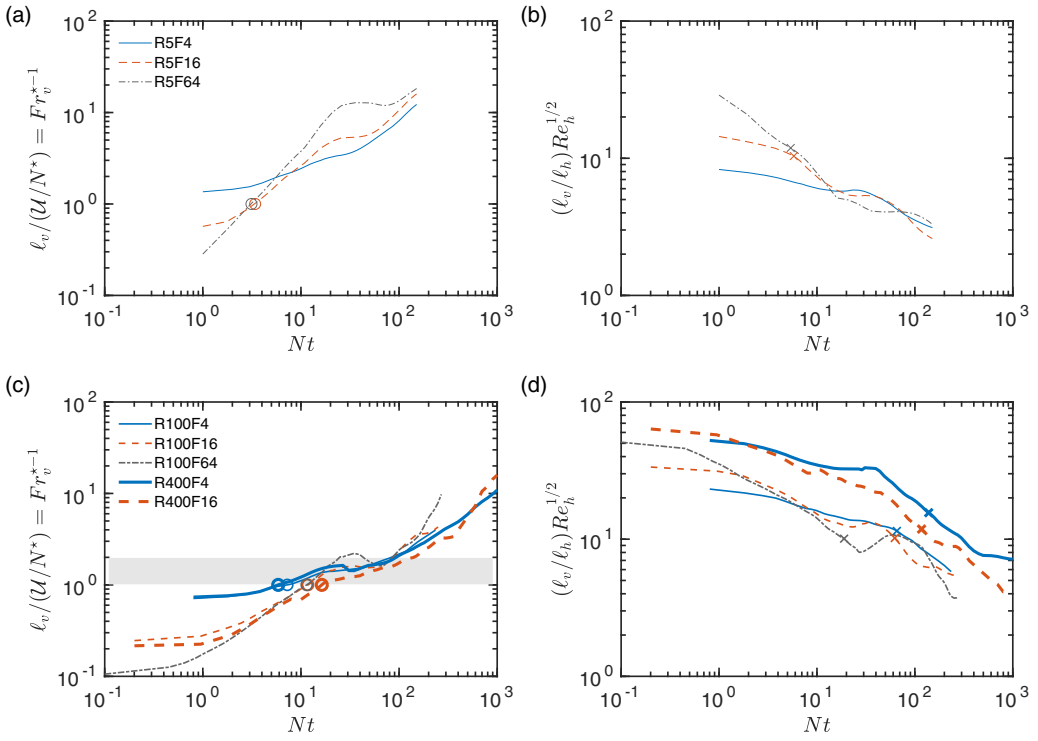

FIG. 7. (a) and (c) Inverse cyclical vertical Froude number $\mathrm{Fr}_v^{\star -1} \equiv \ell_v N^\star/\mathcal{U}$ as a function of time. (b) and (d) Test of the viscous scaling for length scales $\ell_v/\ell_h \sim \mathrm{Re}_h^{-1/2}$. The circles in (a) and (c) mark the unity crossing time of Fr_v^* and the crosses in (b) and (d) mark the unity crossing time of buoyancy Reynolds number $\mathcal{R}$ (Fig. 11). The lightly shaded region in (c) corresponds to $1 < \mathrm{Fr}_v^{\star -1} < 2$, a characteristic dynamical signature of the strongly stratified regime.

$\mathrm{Fr}_v^{\star -1}$, is plotted against the dimensionless time, Nt. On each of the curves (except for R5F4), the instance at which the value of $\mathrm{Fr}_v^\star$ crosses unity is marked with a circle. As discussed in Sec. II B, $\mathrm{Fr}_v^\star = 1$ marks what we define as the entrance into the strongly stratified regime. The R100 and R400 curves [Fig. 7(c)] cross unity within a narrow range of Nt from 6 to 16, and the $\mathrm{Fr}_v^{\star -1}$ values are observed to grow weakly with time within the shaded range of $1 < \mathrm{Fr}_v^{\star -1} < 2$. Within this shaded region, the value of $\mathrm{Fr}_v^\star$ is $O(1)$, which is a dynamical signature of the strongly stratified regime where the inviscid buoyancy scaling of vertical length scale, i.e., Eq. (6), is expected to prevail. Indeed, for these wakes of $\mathrm{Fr}_v^\star$ values of $O(1)$, buoyancy-driven shear layers are observed to dominate the flow (see the R100 and R400 visualizations shown in Figs. 4 and 5). The slow growth of $\mathrm{Fr}_v^{\star -1}$ suggests a possible early stage of the strongly stratified regime, i.e., $10 \lesssim Nt \lesssim 40$, where the flow gradually adapts to the strongly stratified dynamics. Moreover, particularly for the $\mathrm{Fr} = 4$ wakes, $\mathrm{Fr}_v^\star$ remains within the considerably narrow range of 0.61–0.79 during the interval $10 \lesssim Nt \lesssim 40$. The R5 wakes [Fig. 7(a)], on the contrary, continue to grow in $\mathrm{Fr}_v^{\star -1}$ beyond the unity crossing points (the R5F4 values stay above unity for all times), suggesting a different type of dynamics in the R5 wakes from the R100 and R400 wakes.

In Figs. 7(b) and 7(d), the viscous scaling Eq. (7) for the aspect ratio $\ell_v/\ell_h \sim \mathrm{Re}_h^{-1/2}$ is examined. Consistent with the viscous scaling, $(\ell_v/\ell_h)\mathrm{Re}_h^{1/2}$ in the R5 wakes [Fig. 7(b)] quickly attains $O(1)$ values by the time $Nt \sim O(10)$; the smooth and diffused vortical structures dominate the flow thereafter (see the R5 visualizations shown in Figs. 4 and 5). It, however, takes a significantly longer time for the larger-Re wakes [Fig. 7(d)] to approach the viscous regime, i.e., the cross marks ($\mathcal{R} = 1$)

appear at larger values of Nt in Fig. 7(d) than in Fig. 7(b) for a given value of Fr. This is due to the fact that for the R100 and R400 wakes, $(\ell_v/\ell_h)\mathrm{Re}_h^{1/2}$ decreases from much larger initial values in early wakes. The time evolution of the length scales is suggestive of a gradual transition between two distinct (inviscid vs. viscous) scalings (for the R100 and R400 wakes specifically) for ℓ_v and a strong dependence on the wake's Reynolds number, a recurring theme in the remainder of the paper as we analyze various other turbulence diagnostics. No circles or crosses could be drawn for the R5F4 case, because $\mathrm{Fr}_v^* < 1$ [Fig. 9(a)] and $\mathcal{R} < 1$ (Fig. 11) for the entire period of time simulated for this particular wake.

Finally, as discussed in Sec. II B, in Fig. 7(d), $(\ell_v/\ell_h)\mathrm{Re}_h^{1/2} \approx 1$ is not yet attained over the times shown for all higher-Re (R100 and R400) simulations, suggesting that the flows are still transitioning into, and have not fully entered, the viscously dominated regime at these late times. As such, despite values of $\mathcal{R} \approx 1$, one still observes the presence of patchy turbulent fine structure in Fig. 4(c). The full relaminarization of the flow is thus expected at a later time than when $\mathcal{R} \approx 1$.

B. Turbulent velocities

The characteristic turbulent velocities in the stratified wakes are examined in Fig. 8. The velocity scale $\mathcal{U}$ represents the root-mean-square horizontal fluctuation velocity $\sqrt{\langle u'^2 + v'^2\rangle_V^2}$, where $\langle . \rangle_V$ denotes a volume average within the wake's turbulent core as defined by Eq. (C3), and $\mathcal{W} \equiv \sqrt{\langle w'^2\rangle_V^2}$ is the vertical fluctuation velocity. In Fig. 8(a), $\mathcal{U}$ is normalized by the tow-speed U and shown as a function of Nt. Wakes of larger Fr typically correspond to a larger value of $\mathcal{U}/U$ at a given value of Nt and Re. For a fixed Fr, the differences between R100F4 and R400F4 are barely visible. Again, similar to previous figures, the circle on each curve marks the unity crossing time of Fr_v^*, i.e., the entrance time into the strongly stratified for R100 and R400 wakes, and the cross marks the unity crossing time of $\mathcal{R}$, i.e., the entrance into the viscous regime. The time interval of each curve between the circle and the cross for the R100 and R400 wakes corresponds, approximately, to the expected time of residence of the flow in the strongly stratified regime.

The dashed line in Fig. 8(a) represents the theoretical prediction Eq. (B7), i.e., $\mathcal{U} \propto t^{-0.5}$, which is described in Appendix B. The R100 and R400 wakes at $\mathrm{Fr} = 4$ and 16 do not assume the theoretical prediction immediately after the wakes enter the strongly stratified regime. The $\mathcal{U}/U$ values rather decay at a significantly slower rate than $t^{-0.5}$ during this regime, i.e., $Nt \lesssim 40$, which is responsible for the slow growth of $\mathrm{Fr}_v^{\star -1}$ during the same time interval, as observed in Fig. 7(c). Per the associated discussion in Sec. V A, for this subset of simulations (R100 and R400 specifically), it is not unreasonable to regard $\mathcal{U}/U$ as actually assuming a constant value within the window $10 \lesssim Nt \lesssim 40$. Such temporal evolution of $\mathcal{U}/U$ is perhaps not entirely surprising. As discussed in Appendix B, the theoretical analysis underlying the predictive scalings used in this study assumes only the viscous dissipation as the only driver of the kinetic energy budget, i.e., Eq. (B2). In contrast, wakes at such earlier times are expected to have non-negligible shear production [15], which may cause the turbulence to decay at a slower rate. Moreover, power lost to internal wave radiation [17], particularly at Re higher than those considered here, is likely to also play an important role in this context.

As the wakes continue to evolve in the strongly stratified regime, the vertical shear weakens (see Sec. V C) and the decay rate of $\mathcal{U}$ seems to approach the predicted decay rate $t^{-0.5}$ for $Nt \gtrsim 40$ in these wakes (R100 and R400). Incidentally, the decay rate of the R100F64 wake (largest Fr simulated in the present study) in the period of $1 \lesssim Nt \lesssim 20$ is close to the scaling law (dotted line) of $\mathcal{U} \propto t^{-2/3}$ proposed by Spedding *et al.* [7] based on arguments for nonstratified ($\mathrm{Fr} = \infty$) axisymmetric wakes.

As an aside, it is worth comparing the wake results shown in Fig. 8(a) to the equivalent ones for decaying stratified homogeneous turbulence, a flow configuration that has attracted extensive research effort (e.g., [33,38,44–49]). For instance, the grid-turbulence experiments of Praud *et al.* [47] reported a decay rate of $t^{-1.3}$ for the turbulent kinetic energy (dominated by horizontal velocities) which is equivalent to $\mathcal{U} \propto t^{-0.65}$. The numerical simulation of Staquet and Godeferd

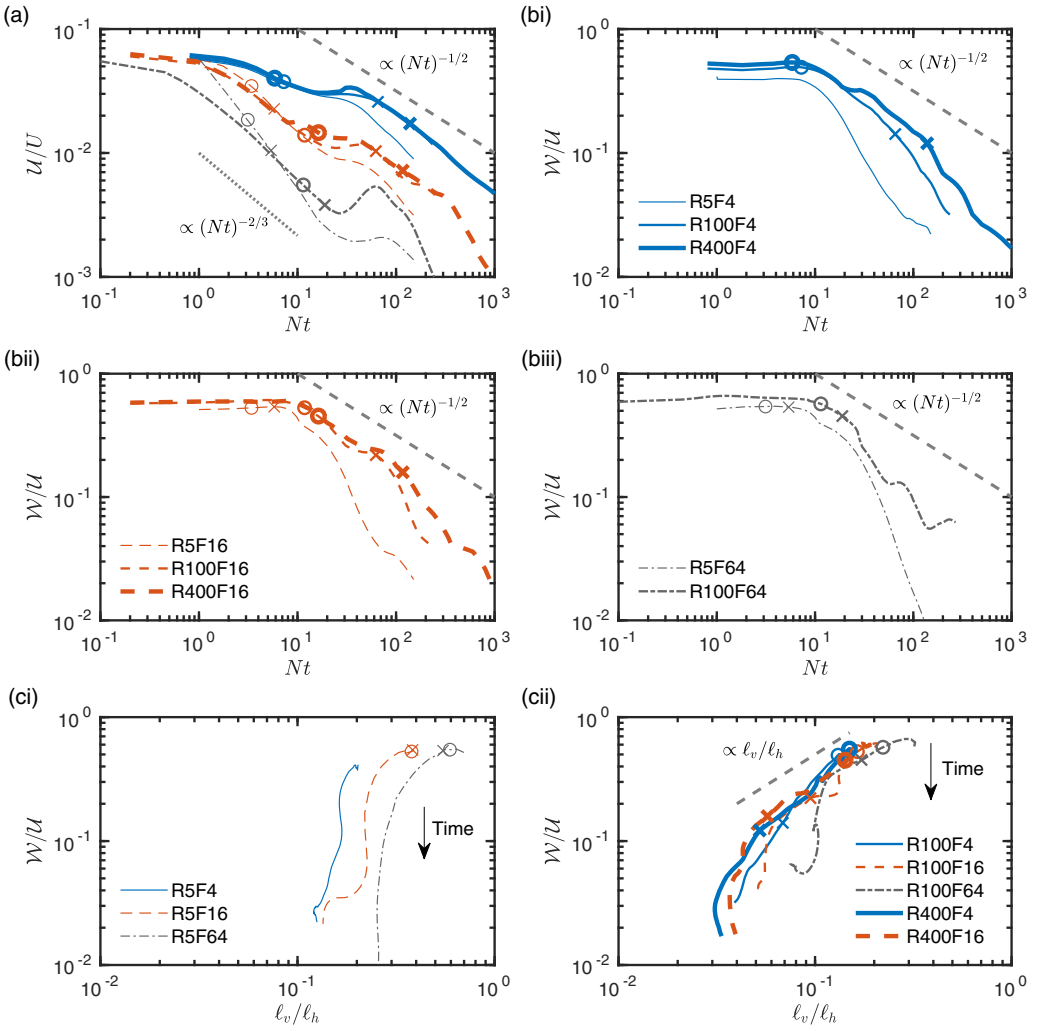

FIG. 8. Time series of (a) $\mathcal{U}/U$ and (b) $\mathcal{W}/\mathcal{U}$, where $\mathcal{U}$ and $\mathcal{W}$ are the horizontal and vertical fluctuation velocities, respectively, and U is the tow speed. (c) Plot of the ratio $\mathcal{W}/\mathcal{U}$ against the length-scale ratio ℓ_v/ℓ_h. Again, the circle on each curve marks the unity crossing time of Fr_v^* and the cross marks the unity crossing time of buoyancy Reynolds number $\mathcal{R}$, a convention that is followed in all subsequent figures. The lines in (a) are identical to those defined in the legends of the other panels.

[49] did observe a decay rate $\mathcal{U} \propto t^{-0.5}$ after the initial flow adjustment to buoyancy (see their Fig. 7), which is identical to the dashed line shown in Fig. 8(a). Very recent simulations of decaying stratified homogeneous turbulence at very high buoyancy Reynolds numbers [37] report decay rates of $\mathcal{U}$ of approximately $t^{-0.56}$.

Figures 8(bi)–8(biii) examine the ratio between $\mathcal{W}$ and $\mathcal{U}$, a first measure of the anisotropy of the turbulence. As is expected for a stably stratified flow, the ratio $\mathcal{W}/\mathcal{U}$ in general decreases with time, indicating a faster decay rate for $\mathcal{W}$ than for $\mathcal{U}$. As the R100 and R400 wakes enter the strongly stratified regime, i.e., for $Nt \gtrsim 10$, wakes of larger Re typically correspond to a larger value of $\mathcal{W}/\mathcal{U}$ at a given value of Nt, similar to the evolution of $\mathcal{U}/U$ shown in Fig. 8(a). The strongly stratified turbulence theory (see, e.g., [30,50]) postulates that by scaling the continuity equation, one is to

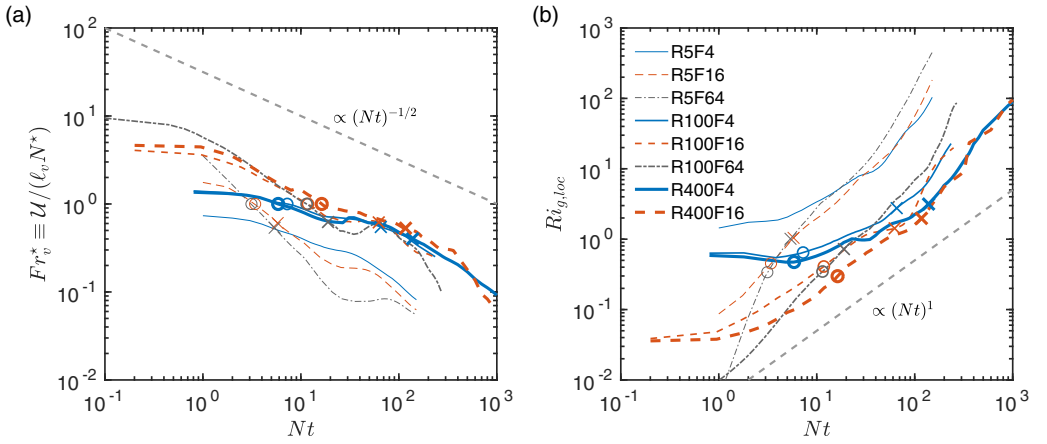

FIG. 9. Time series of (a) the cyclical vertical Froude number $\mathrm{Fr}_v^\star$ and (b) the median local gradient Richardson number $\mathrm{Ri}_{g,\mathrm{loc}}$.

expect

$$\frac{\mathcal{W}}{\mathcal{U}} \sim \frac{\ell_v}{\ell_h}. \tag{11}$$

This suggests that the anisotropy of the flow is determined by the aspect ratio of turbulent flow structure, i.e., ℓ_v/ℓ_h, in order to maintain continuity. The scaling in Eq. (11) for ℓ_v/ℓ_h relies on the continuity argument for the integral scales, which is distinct from the viscous scaling according to Eq. (7). The R100 and R400 wake data appear to be consistent with the above scaling in Eq. (11) when the flow indeed resides in the strongly stratified regime, i.e., the $\mathcal{W}/\mathcal{U}$ values between the circles and crosses [Fig. 8(cii)] vary approximately linearly with the aspect ratio ℓ_v/ℓ_h. In contrast, the values of $\mathcal{W}/\mathcal{U}$ drop off much more quickly beyond the crosses on these curves, indicating a faster decay rate for $\mathcal{W}$ in the viscous regime.

C. Local vertical shear

Central to the dynamics of strongly stratified turbulence is the decoupling of the coherent horizontal motions in the vertical direction causing vertical shearing between layers to trigger shear instabilities that lead to small-scale turbulence, e.g., as first discussed by Lilly [22]. To characterize the tendency of forming local shear instabilities, we examine the local gradient Richardson number $\mathrm{Ri}_{g,\mathrm{loc}}$ as defined by

$$\mathrm{Ri}_{g,\mathrm{loc}} \equiv \frac{-\frac{g}{\rho_0}\frac{\partial \rho_T}{\partial z}}{\left(\frac{\partial u}{\partial z}\right)^2 + \left(\frac{\partial v}{\partial z}\right)^2}, \tag{12}$$

where the total density $\rho_T(x, y, z, t) = \overline{\rho}(z) + \rho'(x, y, z, t)$. Such a local Richardson number is commonly used in the stratified turbulence literature (e.g., [26,51]). In the context of stratified wakes, the $\mathrm{Ri}_{g,\mathrm{loc}}$ values are first sampled locally within the turbulent wake core, i.e., as defined by Eq. (C3), and the median value of all local samples at each time is examined in Fig. 9. The squared local vertical shear in Eq. (12) is expected to scale as

$$\mathcal{S}^2 \equiv \left(\frac{\partial u}{\partial z}\right)^2 + \left(\frac{\partial v}{\partial z}\right)^2 \sim \left(\frac{\mathcal{U}}{\ell_v}\right)^2 \tag{13}$$

and the total buoyancy gradient in Eq. (12) is expected to scale as N^2. Therefore,

$$\mathrm{Ri}_{g,\mathrm{loc}} \sim \left(\frac{\ell_v N}{\mathcal{U}}\right)^2 = \mathrm{Fr}_v^{-2}. \tag{14}$$

It should be noted that the above scaling is a generic one that is expected to hold for a wide range of stratified flows, not limited to the strongly stratified regime. Noting that $\mathcal{U} \propto t^{-0.5}$ and $\ell_v \propto t^0$ (see Appendix B), one expects the following time dependence for Fr_v and $\mathrm{Ri}_{g,\mathrm{loc}}$, respectively:

$$\mathrm{Fr}_v \propto t^{-0.5}, \quad \mathrm{Ri}_{g,\mathrm{loc}} \propto t. \tag{15}$$

The latter scaling implies that the buoyancy-driven shear layers are expected to become stabilized in time as the local gradient Richardson number increases. This stabilization is due to the fact that the turbulent velocity $\mathcal{U}$ decays in time while the vertical length scale ℓ_v stays approximately constant, which together cause the local vertical shear $\mathcal{S}$ to weaken.

The time series of $\mathrm{Fr}_v^\star \equiv 2\pi\,\mathrm{Fr}_v$ and the median $\mathrm{Ri}_{g,\mathrm{loc}}$ values are shown, respectively, in Figs. 9(a) and 9(b) for all wakes simulated. Apart from the potential existence, earlier in the strongly stratified regime, of the transitional, short-duration interval of slowly decaying $\mathrm{Fr}_v^\star \approx O(1)$, discussed in Sec. V A, the time series do approach the expected power-law slopes in Eq. (15) by $Nt \simeq 50$ for the R100 and R400 wakes. We reiterate here that any power-law scaling involving time discussed in this paper is not rooted within the fundamental underlying assumptions associated with strongly stratified turbulence but rather in the theory of decaying homogeneous stratified turbulence as reviewed in Appendix B. The applicability of these power laws is strictly for the wake flow under consideration only, not for any stratified turbulence in general. The F16 wakes start to follow the predicted scaling at an earlier time, which is likely an artifact of the wake initialization scheme (see [10]). The median value of $\mathrm{Ri}_{g,\mathrm{loc}}$ lies between 0.30 and 0.65 as the wakes enter the strongly stratified regime, and exit values (marked by crosses) vary with the wake Reynolds number, i.e., higher-Re wakes leave the strongly stratified regime at a larger median $\mathrm{Ri}_{g,\mathrm{loc}}$ than the lower-Re wakes. The R5 wakes do exhibit significantly larger values of $\mathrm{Ri}_{g,\mathrm{loc}}$ than those in the R100 and R400 wakes throughout the wake's life cycle, which is consistent with the absence of disturbances within the shear layers in R5 wakes [Fig. 5(a)].

Such a difference in the stability of the shear layers is fundamentally linked to the selection mechanism for the vertical scale ℓ_v in the strongly stratified regime and in the viscous regime, respectively, as discussed in Sec. II and in Sec. V A: Within the wakes (R100 and R400) which enter the strongly stratified regime after the initial adjustment to buoyancy, ℓ_v spontaneously adjusts to match the $\mathcal{U}/N$ scaling such that $\mathrm{Fr}_v^* \sim O(1)$, and hence $\mathrm{Ri}_{g,\mathrm{loc}}$ remains $O(1)$ as well, continuing to support instabilities to develop within the shear layers [Figs. 5(b) and 4(c)]; for the wakes (R5) transitioning directly into the viscous regime, ℓ_v adjusts to match the viscous scaling instead, i.e., $(\ell_h/\ell_v)\mathrm{Re}_h^{1/2} \sim O(1)$ [Fig. 7(b)], resulting in larger ℓ_v/D [Fig. 6(a)], smaller Fr_v^* [Fig. 9(a)], and larger $\mathrm{Ri}_{g,\mathrm{loc}}$ [Fig. 9(b)], as compared to their R100 and R400 counterparts. In these R5 wakes which do not access the strongly stratified regime, stable shear layers dominate the flow by $Nt \simeq 10$ and quickly laminarize [see, e.g., Fig. 5(a)]. The particular scaling that $\mathrm{Fr}_v^* \sim O(1)$, which holds for a prolonged period of time in the R100 and R400 wakes and allows for shear instability to occur within the layered flow structure, is a defining feature of the strongly stratified regime (see, e.g., [24,30,33,50]).

VI. STRATIFIED FLOW REGIMES AND TRANSITIONS

A. Turbulent Reynolds- and Froude-number phase space

With the evolution of individual turbulence quantities now examined in Sec. V, we move forward in this section with investigating some relevant dimensionless parameters and the trajectories these parameters form in the corresponding phase spaces. In Fig. 10, the time series of the horizontal turbulent Reynolds and Froude numbers Re_h and Fr_h, respectively, defined in Eq. (1), are shown.

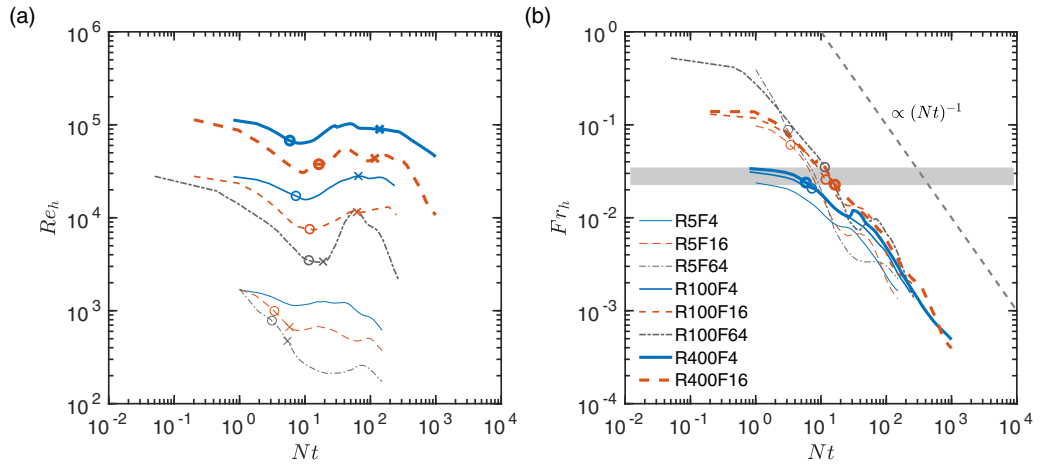

FIG. 10. Variation of horizontal turbulence Reynolds and Froude numbers Re_h and Fr_h, respectively, with the dimensionless time Nt. The shaded region is (b) corresponds to $0.021 < \mathrm{Fr}_h < 0.035$, the range of Fr_h values at which the wakes enter the strongly stratified regime.

The time series of Re_h in Fig. 10(a) show an initial decrease with time in early wakes up to $Nt \simeq 10$. For the R5 wakes which do not access the strongly stratified regime (with $\mathcal{R} > 1$ and $\mathrm{Fr}_h \ll 1$), the decreasing trend appears to carry on. However, for the R100 and R400 wakes which indeed access the strongly stratified regime, Re_h becomes relatively constant in time during the strongly stratified regime (between the circles and crosses on each curve), an observation that motivates our scaling predictions in Eq. (B7). That the wakes accessing the strongly stratified regime appear to maintain a constant (or at least same order of magnitude) value of Re_h is a result of the decay of fluctuation velocity $\mathcal{U}$ [Fig. 8(a)] being compensated by the growth of length scale ℓ_h [Fig. 6(d)]. The R100F64 wake exhibits some significant fluctuations in Re_h upon exiting from the strongly stratified regime, which is likely associated with vortex merging events during the viscous regime which are not the focus of this study.

As an aside, Spedding *et al.* [52] reported a scaling of $t^{-1/3}$ for a local Reynolds number computed for laboratory stratified wakes of Re up to 10^4. A direct comparison of this Reynolds number with the data reported in Fig. 11(a) is perhaps not informative, because the mean-flow component was included in calculating the velocity scale considered by Spedding *et al.* [7], while the velocity scale $\mathcal{U}$ considered here only includes the fluctuation turbulent velocities, so the resulting Re_h and Fr_h estimates are analogous to their counterparts defined for homogeneous turbulence without mean flows.

Figure 10(b) shows the evolution of Fr_h in time. The initial values of Fr_h in early wakes are strongly dependent on the body-based Froude number Fr, but such a dependence largely vanishes by $Nt \sim O(10)$. The Fr_h values at which the R100 and F400 wakes enter the strongly stratified regime (marked by circles) fall in a considerably narrow range of 0.021–0.035 (highlighted in gray). The power-law decay rate of Fr_h approaches t^{-1} (gray dashed line) as the wakes evolve into the strongly stratified regime ($Nt \gtrsim 40$), consistent with the prediction of Eq. (B6). This suggests that the assumptions behind this particular scaling, i.e., Taylor's estimate as in Eq. (B1) and the dominance of viscous dissipation in the turbulent kinetic energy budget as in Eq. (B2), might indeed be valid in stratified wakes for $Nt \gtrsim 40$ (see the discussion in Appendix B). That Fr_h decays as t^{-1} is also consistent with the evolution of local Froude number in experiments of Spedding *et al.* [7], even though their definition of velocity scale is different from that of the present study.

Figure 11 shows the trajectories followed by each of the eight wake simulations in the parameter space formed by Re_h and Fr_h^{-1} [24]. The five simulations for the two larger Re values do access the strongly stratified regime. The transition boundary from the weakly stratified to strongly stratified

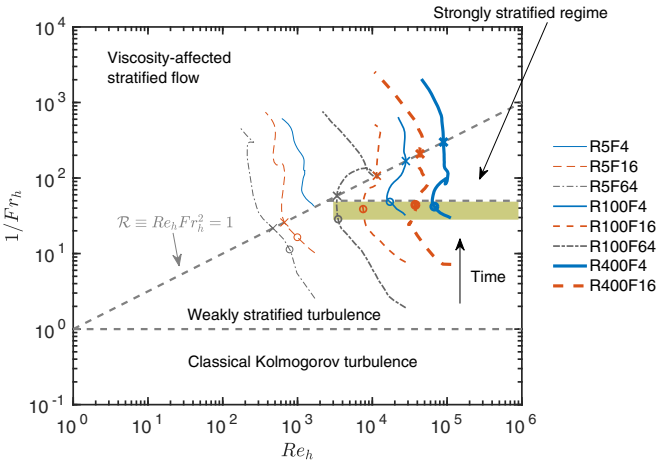

FIG. 11. Trajectories followed by stratified wakes in the parameter space formed by Re_h and Fr_h^{-1} [24]. Circles mark the times at which the vertical Froude number $\mathrm{Fr}_v^\star$ becomes unity, i.e., $\mathrm{Fr}_v^{\star\dagger} \equiv 1$, and crosses mark when the buoyancy Reynolds number $\mathcal{R}$ becomes unity, i.e., $\mathcal{R}^\ddagger \equiv 1$. The shaded region corresponds to $29 < \mathrm{Fr}_h^{-1} < 48$, the range of Fr_h^{-1} values at which the wakes enter the strongly stratified regime.

regime is represented by the horizontal dashed line corresponding to $\mathrm{Fr}_h = 0.02$, the threshold value predicted by Lindborg [25]. The entrance into the strongly stratified regime for wakes, based on the very definition of Eq. (9), occurs at Fr_h values fairly close to (slightly larger than) 0.02 [see the shaded region in Fig. 10(b) or in Fig. 11] as indicated above. However, this resemblance may simply be fortuitous as the numerical values of Fr_h could change considerably depending on the specific definitions of length scales and velocity scales, and the threshold value may well be dependent on the chosen definition of this transition, i.e., Eq. (9).

As shown in Fig. 11, the R5 wakes transition directly from the weakly stratified turbulence regime to the viscous regime, i.e., the Fr_h value is never sufficiently small before the flow becomes viscously dominated. For R100 and R400 wakes which do access the strongly stratified regime, the trajectory shifts to the right (along the Re_h axis) with either larger Re or smaller Fr. As it shifts to the right, a longer fraction of the trajectory resides within the strongly stratified regime (the portion between the circle and the cross), accessing smaller value of Fr_h before leaving the strongly stratified regime to enter the viscous regime. Such quantitative effects of Re and Fr on these trajectories are discussed further in Sec. VI B.

B. Dependence on stratified wake parameters

The strongly stratified regime requires $\mathcal{R} \equiv \mathrm{Re}_h \mathrm{Fr}_h^2 > 1$ and $\mathrm{Fr}_h \ll 1$ concurrently. Here we attempt to develop a predictive capability for whether the wake turbulence can access the strongly stratified regime, given the wake's externally specified body-based parameters Re and Fr. As is shown in Fig. 11, Re and Fr have a significant impact on the Re_h value at which a stratified wake enters the strongly stratified regime, i.e., $\mathrm{Re}_h^\dagger$. On the other hand, the initial values of the horizontal Froude number upon the entry into the strongly stratified regime fall within the relatively narrow range of $0.021 < \mathrm{Fr}_h^\dagger < 0.035$. We will further assume that the value of $\mathrm{Fr}_h^\dagger$ is a generic property of stratified turbulence and does not vary with body-based Re and Fr; specifically, we will set

$$\mathrm{Fr}_h^\dagger = \mathrm{const} \simeq 0.02, \tag{16}$$

following the estimate of Lindborg [25] [see his Eq. (21)], which seems to provide a lower (more conservative) bound for the observed $\mathrm{Fr}_h^\dagger$ values shown in Fig. 11. For a wake to access the strongly stratified regime, the requirement is that the value of $\mathcal{R}$ is still above order unity at the point when

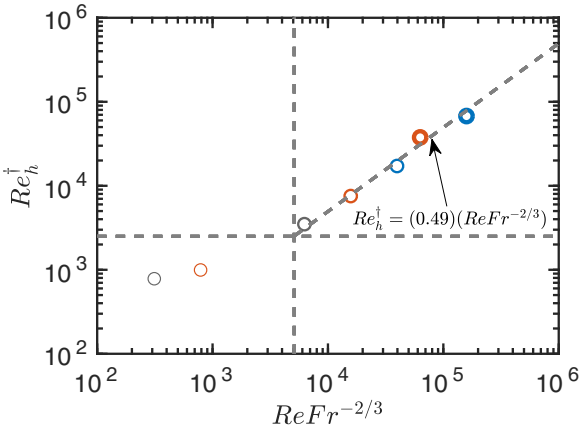

FIG. 12. Transitional horizontal turbulent Reynolds number $\mathrm{Re}_h^\dagger$ as the flow enters the strongly stratified regime and its dependence on the wake's body-based parameters Re and Fr. The horizontal line corresponds to the lower bound of $\mathrm{Re}_h^\dagger$ in order for the wake to access the strongly stratified regime, according to Eq. (17). The vertical line corresponds to the threshold value of $\mathrm{Re}\,\mathrm{Fr}^{-2/3}$ for wakes accessing the strongly stratified regime, according to Eq. (22).

Fr_h becomes small enough, i.e., $\mathcal{R}^\dagger > 1$ when $\mathrm{Fr}_h = \mathrm{Fr}_h^\dagger$, or equivalently

$$\mathrm{Re}_h^\dagger > \frac{1}{\mathrm{Fr}_h^{\dagger 2}} \simeq 2.5 \times 10^3, \tag{17}$$

which provides a threshold value for $\mathrm{Re}_h^\dagger$ in order for a wake to enter the strongly stratified regime. In order to express $\mathrm{Re}_h^\dagger$ as a function of Re and Fr, we employ the mean-flow-based wake scalings reported by Spedding [5]. The $\mathrm{Re}_h^\dagger$ can be rewritten as

$$\mathrm{Re}_h^\dagger \equiv \frac{\mathcal{U}^\dagger \ell_h^\dagger}{\nu} = \frac{\mathcal{U}^\dagger}{U}\frac{\ell_h^\dagger}{D}\mathrm{Re}, \tag{18}$$

where $\mathcal{U}^\dagger \equiv \mathcal{U}(t = t^\dagger)$ and $\ell_h^\dagger \equiv \ell_h(t = t^\dagger)$. It is observed in our simulations that $Nt^\dagger$ falls in a relatively narrow range $6 < Nt^\dagger < 16$ (see, e.g., Fig. 10), a subwindow within the NEQ regime ($2 < Nt < 50$) where the wake's centerline velocity U_0 varies relatively slowly with t [see, e.g., Fig. 7(a) of [10]]. In order to proceed, we further approximate $Nt^\dagger$ to be a constant across all values of Re and Fr. Given that the turbulent velocity $\mathcal{U}$ follows the same Fr scaling as U_0 (see, e.g., [5,7]), we obtain

$$\frac{\mathcal{U}^\dagger}{U} \sim \frac{U_0(t = t^\dagger)}{U} \propto \mathrm{Fr}^{-2/3}, \tag{19}$$

where the latter proportionality between U_0/U and Fr has been reported by numerous experimental (e.g., [1]) and numerical (e.g., [10,20]) studies. It is also observed that the $\ell_h^\dagger/D$ value has little dependence on Re or Fr, as shown in Fig. 6(d). Therefore, one can deduce from Eqs. (18) and (19) that

$$\mathrm{Re}_h^\dagger \propto \mathrm{Re}\,\mathrm{Fr}^{-2/3}. \tag{20}$$

In Fig. 12 we test the scaling of Eq. (20) between $\mathrm{Re}_h^\dagger$ and $\mathrm{Re}\,\mathrm{Fr}^{-2/3}$. Our numerical data match this scaling prediction reasonably well for larger values of $\mathrm{Re}\,\mathrm{Fr}^{-2/3}$. In particular, we find empirically (via a least-squares fit) that

$$\mathrm{Re}_h^\dagger \simeq (0.49)(\mathrm{Re}\,\mathrm{Fr}^{-2/3}) \tag{21}$$

for simulations which actually access the strongly stratified regime (see Fig. 12). Substituting Eq. (21) into Eq. (17), one can find a (minimum) threshold value for $\mathrm{Re}\,\mathrm{Fr}^{-2/3}$ which is required for a wake to access the strongly stratified regime, i.e.,

$$\mathrm{Re}\,\mathrm{Fr}^{-2/3} \gtrsim 5 \times 10^3. \tag{22}$$

This effectively provides a quantitative tool to predict the relevance of the strongly stratified regime for a geophysical or naval wake [1] of given Re and Fr.

VII. CONCLUSION

We have examined the structural and dynamical characteristics of the turbulence in stratified towed-sphere wakes, a canonical turbulent free-shear flow, using the framework of the strongly stratified turbulence theory (as reviewed in Sec. II) and a recent large-eddy simulation data set (Sec. III). With further theoretical considerations made in the context of wakes (Sec. II B and Appendix B) and the basic phenomenology presented (Sec. IV), we examine the large-scale turbulence characteristics, such as length and velocity scales and the associated nondimensional parameters (Sec. V), focusing on their time evolution as the wake progresses through various regimes (Fig. 11). Our simulations have revealed significant effects of the wake's body-based Reynolds number Re on the evolution of wake turbulence. In particular, we have gained the capability of predicting whether a wake at a particular value of body-based Re and Fr could access the strongly stratified regime (Sec. VI B) in which the dynamics are dominated by anisotropic layerwise structures in the vertical which are prone to shear instability (Sec. V C). Specifically, for a given wake, the value of $\mathrm{Re}\,\mathrm{Fr}^{-2/3}$ is required to exceed a threshold value of approximately 5×10^3 (Fig. 12) in order for the wake turbulence to access the strongly stratified regime. This result provides a criterion for assessing the relevance of the strongly stratified dynamics for geophysical and naval wakes (see, e.g., [1]) which typically have large Reynolds numbers $\mathrm{Re} \sim O(10^8)$–$O(10^9)$ and a wide range of large Froude numbers $\mathrm{Fr} \sim O(10^{-1})$–$O(10^3)$. The effects of Re were quantitatively and systematically discussed in the context of the towed-sphere stratified wake, an inhomogeneous, freely evolving (i.e., unforced), localized turbulent shear flow, with a focus on the associated dynamics of strongly stratified turbulence.

This study constitutes a systematic examination of stratified wake turbulence at three distinct Re values sufficiently separated in magnitude. As shown in Fig. 11, the wakes of $\mathrm{Re} = 5 \times 10^3$ (lowest value examined here) never access the strongly stratified regime, rapidly entering the viscously dominated flow regime from the weakly stratified regime. Wakes at $\mathrm{Re} = 10^5$ and 4×10^5 do access the strongly stratified regime, e.g., as evidenced in Fig. 11. While it is observed that the R100 and R400 wakes may exhibit similar statistics, e.g., the R100 and R400 curves seem to collapse for the vertical integral scale ℓ_v in Fig. 6(c) and for horizontal fluctuation velocity $\mathcal{U}$ in Fig. 8(a), it might still be premature to claim that an asymptote in Re has been reached in terms of those statistics, given the perhaps still limited quadruple increase in Re from R100 to R400 that is computationally feasible in the present study. Simulations at even higher Re, which effectively allow one to access higher $\mathcal{R}$ and lower Fr_h simultaneously, are needed to further assess the sensitivity of strongly stratified dynamics to Reynolds number in the geophysically relevant range [1,29]. In terms of the turbulent energetics, we observe an early-stage transitional period of the strongly stratified regime, i.e., $10 \lesssim Nt \lesssim 40$, for which we anticipate that shear production and internal wave radiation are also relevant contributors to the energy budget, other than viscous dissipation which indeed dominates the budget for $Nt \gtrsim 40$. These additional dynamics, such as internal wave radiation, have been found to be sensitive to Re [17–19]. Consequently, potential adaptations to the energetics considerations (Appendix B) to account for additional energy sources and sinks could be relevant at even higher Re values, which are currently limited by computational resources to investigate.

Another intriguing aspect of even higher Re is its potential modification to the turbulent flow structures, which is critically linked to the competing selection mechanisms for the vertical integral

scale ℓ_v (Sec. V A) and the implications for the stability properties of the buoyancy-driven shear layers (Sec. V C). The results presented here (Figs. 4 and 5) have revealed some qualitative effects of Re on the spatial density and the longevity of shear instabilities between buoyancy-driven layered structures [23]. Per the scaling in terms of Re developed in Sec. VI B for stratified wakes and recent observations in DNSs of stratified homogeneous turbulence (e.g., [37]) at sufficiently low values of Fr_h and higher values of buoyancy Reynolds number than those attained for wakes in the present study, it is reasonable to expect that in higher-Re stratified wakes, highly anisotropic energetic turbulence can be present in an even larger spatial fraction of wake core, at a time that is well into a further prolonged strongly stratified regime, i.e., $Nt \sim O(100)$ or even higher. Spatially localized and temporally intermittent turbulent bursts, originating from buoyancy-driven shear instabilities, are expected to continue at even later times.

Several other avenues for future research arise from the present study. From the turbulence modeling perspective, it is imperative to incorporate high-Re strongly stratified dynamics into the self-similarity modeling paradigm for stratified wakes established by Spedding [5]. In the analysis presented in this paper, we have focused on volume-averaged statistics within the wake core assuming that the statistics are almost quasihomogeneous; the inhomogeneous aspects of the wake flow await further study. For instance, given the degree of inhomogeneity (see, e.g., [19]) of turbulence within the wake, the uniform-eddy-diffusivity assumption made in the self-similarity model of Meunier *et al.* [53] might not be appropriate for geophysically relevant parameter ranges and thus needs to be adapted accordingly. Moreover, particularly for Re values higher than those considered here, this eddy diffusivity is likely to have a non-negligible vertical component well into the strongly stratified regime, in contrast to the assumption made in Ref. [53] that all vertical momentum transport ceases after $Nt \approx 2$.

From a dynamical perspective, it is intriguing to explore how the coherent pancake vortices (Fig. 4) are modified by further increasing Re: Do these structures ever form and remain robust at geophysically relevant values of Re, at least over timescales of practical interest? What is the exact dynamical pathway (see, e.g., [54]) for the turbulence to evolve, spatially or temporally, from the near-wake three-dimensional turbulent state within the weakly stratified turbulence regime to the highly anisotropic layered state within the strongly stratified regime? Is the zigzag instability mechanism associated with vortex pairs and/or horizontal shear [6,51,55–59] operative in wakes of larger Re where the horizontal motions are becoming much less coherent (Fig. 4)? From an oceanographic perspective, it is interesting to examine the irreversible mixing characteristics in strongly stratified turbulence, taking into account the potential effects of the formation of layered density structures which requires large values of buoyancy Reynolds number and gradient Richardson number concurrently [60,61]. Finally, the numerical data set used in this paper has also served as a platform to explore the energetics of turbulence-driven internal wave radiation by high-Re wakes, the subject of a separate study [17].

ACKNOWLEDGMENTS

Support from Office of Naval Research through Grants No. N00014-13-1-0665 and No. N00014-15-1-2513 is gratefully acknowledged. High-performance computing resources were provided through the U.S. Department of Defence High Performance Computing Modernization Program by the Army Engineer Research and Development Center and the Army Research Laboratory under Frontier Project No. FP-CFD-FY14-007. We thank Professor J. Riley, Professor S. de Bruyn Kops, Professor G. Spedding, and Dr. A. Muschinski for illuminating discussions on stratified turbulence and Professor S. Pope for carefully commenting on preliminary results presented in Ref. [20]. Dr. K. Rowe is acknowledged for meticulously converting a large volume of raw simulation data to a more accessible format for the analysis reported in this paper. The work of Q.Z. was supported in part by UK EPSRC Program Grant No. EP/K034529/1 entitled "Mathematical Underpinnings of Stratified Turbulence" awarded to the University of Cambridge and by the Natural Sciences and Engineering Research Council of Canada Discovery Grant No. RGPIN-2018-04329. Additional computing

resources were enabled in part by Compute Canada and by the University of Calgary. We thank an anonymous referee for many constructive comments which improved the quality of the paper.

APPENDIX A: ADDITIONAL INFORMATION ON NUMERICAL CONFIGURATION

In this Appendix we review some numerical aspects of the stratified wake simulations reported in this paper. In particular, we examine the specific choices of grid resolution and spectral filters aimed to ensure adequate resolution of the flow physics while maintaining numerical stability. As discussed in Sec. III of this paper and Sec. 2.5 of [10], the ILES solver [9] does not explicitly implement a particular subgrid-scale model. Instead, spectral filtering is applied directly to the flow field to drive the downscaled energy flux in the unresolved scales and prevent spectral blockage at the smallest resolved scales. Spectral filtering is applied to both Fourier-discretized horizontal directions and to the Legendre-multidomain-discretized vertical direction. For ease of discussion, we will focus on the horizontal directions, as the relation between a Fourier mode and the corresponding length scale can be more directly established. Moreover, the discussion will be restricted to a one-dimensional filter in the periodic x direction. The main conclusions of this discussion may then be translated to the actual isotropic two-dimensional filter used on the Fourier-discretized horizontal plane in this study (see Sec. 2.4 of [10]).

The particular filter function used in this study consists of a transfer function $\hat{G}$ [62] of an exponential form. In the case of the periodic x direction, where N_x grid points correspond to $N_x/2$ complex Fourier modes, the spectral filter may be written as

$$\hat{G}(k) = \exp\left[-\alpha\left(\frac{\tilde{k}}{\tilde{N}}\right)^p\right], \tag{A1}$$

where $\tilde{k} = 0, 1, \ldots, \tilde{N}$ is the mode number or modal index and $\tilde{N} = N_x/2$ is the largest modal index corresponding to the grid resolution. In addition, $\alpha = -\ln \epsilon_M$ (ϵ_M is the machine epsilon) and p is the filter order (typically an even integer). It is of interest to define a cutoff wave number k_c, e.g., after (13.14) of Ref. [62],

$$k_c \equiv \frac{\pi}{\Delta}, \tag{A2}$$

a wave number above which the transfer function drops below 0.99, i.e.,

$$\hat{G}(k \geqslant k_c) \leqslant 0.99. \tag{A3}$$

In other words, Δ is the cutoff (or transitional) length scale between scales that are not significantly impacted by the filter ($\hat{G} > 0.99$) and scales that are under stronger impact of the filter ($\hat{G} < 0.99$); Δ is also referred to as the turbulence-resolution length scale [63].

Two additional length scales may then be defined: $\mathcal{L}$, the characteristic length of the flow geometry (for this particular study, $\mathcal{L} \sim D$, where D is the sphere diameter), and h, the grid spacing. The selection of an appropriate cutoff length scale Δ requires that one optimize two length-scale ratios Δ/D and Δ/h. According to Sec. 13 of Ref. [62], it is desirable to minimize Δ/D to retain most of the energy within the nonfiltered component of the resolved scales in the flow field. At the same time, one aims to maximize Δ/h such that the subfilter component of the flow field, i.e., the filtered component of the resolved scales, is adequately resolved to ensure a numerically accurate and stable simulation. Specifically, a sufficiently large value of Δ/h is required for the solution to be independent of the choice of h (see, e.g., [63]).

The aforementioned guidelines are taken into account when the spectral filter functions are prescribed for the simulations of $\mathrm{Re} \in \{5 \times 10^3, 10^5, 4 \times 10^5\}$. The spectral transfer functions $\hat{G}$ used at each of these three Re are plotted as a function of $k_x D$ in Fig. 13(a) and as a function of $k_x h$ in Fig. 13(b). By adjusting, as needed, the values of $\tilde{N}$ and p in Eq. (A1), one sets the cutoff wave number k_c and consequently sets the ratios Δ/D and Δ/h. On the one hand, added resolution (larger $\tilde{N}$ and smaller h) for increasing Re (Table I) ensures a sufficiently small Δ/D ratio value,

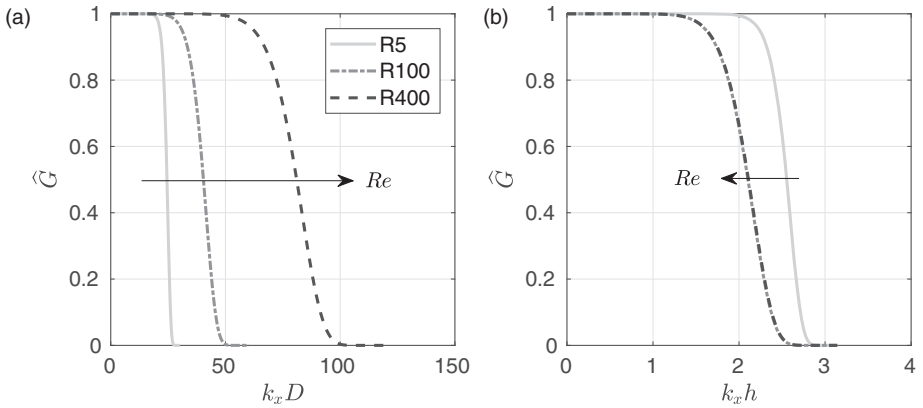

FIG. 13. Transfer function $\hat{G}$ as a function of (a) $k_x D$ and (b) $k_x h$ for simulations at Re $\in \{5 \times 10^3, 10^5, 4 \times 10^5\}$. The dimensionless cutoff wave number $k_c D$ (as measured by the wave number at which $\hat{G}$ drops to 0.99) is 19.8, 26.2, and 53.0 for the three Re values, respectively, corresponding to Δ/D ratios of 0.16, 0.12, and 0.059. The value of $k_c h$ is 2.06, 1.38, and 1.38 for the three Re values, corresponding to Δ/h ratios of 1.5, 2.3, and 2.3.

i.e., $\{0.16, 0.12, 0.059\}$ for R5, R100, and R400, respectively. As a result, a significant fraction of the inertial subrange lies above the filter scale (Fig. 14) with this subrange supported by increasing wave number coverage as Re is increased, particularly when moving from R100 to R400. On the other hand, for the purpose of securing a sufficiently large Δ/h ratio for numerical accuracy and stability, a stronger filter, corresponding to lower values of p in Eq. (A1), is used for the two larger values of Re (Fig. 14); in both of these runs the degree of underresolution is expected to be higher than the lowest Re considered in this study. It was recommended by Pope [63] that $\Delta/h \geqslant 4$ for a scheme with second-order spatial accuracy and $\Delta/h \geqslant 2$ for a sixth-order scheme, in order to remove the dependence of the solution on h [64,65]. For the wake simulations considered here, a Δ/h ratio of 1.5 is used for R5, and 2.3 is used for both R100 and R400 [Fig. 13(b)]. These values

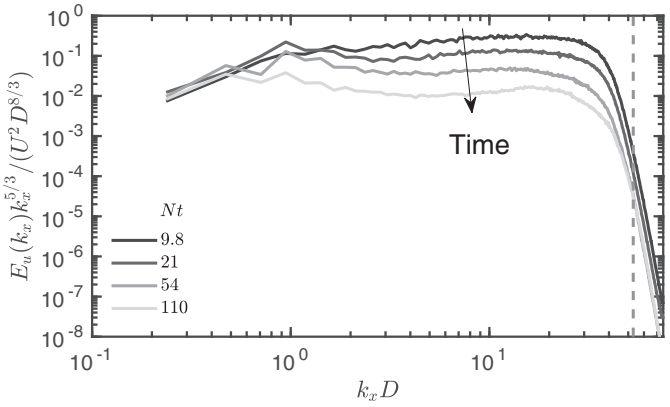

FIG. 14. Sample compensated energy spectrum of the streamwise velocity u for various Nt values from the R400F4 wake. The vertical dashed line indicates the cutoff wave number $k_c D \simeq 53$ beyond which the numerical solutions are directly affected by the Fourier filter (Fig. 13). The spectrum is first sampled pointwise for (y, z) locations within the wake core defined by Eq. (C3) and then averaged over all (y, z) locations sampled to yield the wake-averaged spectrum.

are expected to be sufficient, given the spectral accuracy brought to the specific numerical scheme by the Fourier and Legendre discretizations [9].

Spectral filtering is also applied to the Legendre modal expansions of order $\hat{N}$ within each subdomain in the vertical direction. Two measures are taken to ensure adequate resolution in the vertical. First, smaller subdomains are allocated around the wake centerline at $z = 0$ (see Fig. 3), leveraging the flexibility brought by the multidomain approach. Second, the number of grid points is adjusted through the number of subdomains M and the order of polynomial approximation $\hat{N}$ (see Fig. 3) to provide better resolution at increasing values of Re. For $\mathrm{Re} \in \{5 \times 10^3, 10^5\}$, no fewer grid points in the vertical are used in the present study than in the simulations of [10] for the same wake parameters. For $\mathrm{Re} = 4 \times 10^5$, the vertical resolution is doubled from the $\mathrm{Re} = 10^5$ case, after the anticipated $\mathrm{Re}^{-1/2}$ scaling of the vertical scale of turbulence proposed by Riley and de Bruyn Kops [26]. This increase in vertical resolution is adhered to even if simulation results suggest that the vertical turbulence length scale ℓ_v becomes rather insensitive to Re for $\mathrm{Re} \geqslant 10^5$, as shown in Fig. 6(c).

In configuring these simulations, particular effort is made to ensure that sufficient numerical resolution is provided to adequately capture the dependence of wake physics on Re. The vertical resolution of the wake core is comparable to that used in the DNSs of Watanabe *et al.* [19] (from [43]). Specifically, at $\mathrm{Fr} = 4$ where buoyancy most strongly focuses the shear layers acting as the primary drivers of turbulence in the strongly stratified regime, 26, 60, and 140 points are used for resolution across a vertical integral scale ℓ_v at R5, R100, and R400 respectively. In the horizontal direction, limitations of computational resources and the uniform grid associated with a Fourier discretization prevent attaining DNS-like resolution, i.e., capturing scales comparable to the Kolmogorov scale. Nevertheless, a significant fraction of the turbulent scales of motion is captured, particularly during the strongly stratified regime (if it exists). As shown in the analysis of Diamessis *et al.* [66] and summarized in Sec. 2.5 of [10], over the resolved scales not directly impacted by the spectral filter, the molecular viscosity ν is considerably larger than the numerical viscosity associated with spectral filtering. The numerical viscosity gradually becomes the dominant source of damping only over scales where the spectral filter function drops to values less than unity (Fig. 13).

Further support towards the negligible role of the numerical viscosity over the majority of the resolved scales of the ILES is provided by the comparison of ILES spectra with the corresponding DNS spectra of Watanabe *et al.* [19] at specific times in the strongly stratified regime for the R400F4 case (see Appendix D of Ref. [20]): Up to the wave number where the filter transfer function drops below unity, DNSs and ILESs are in excellent agreement, and it is indeed over these unfiltered scales that the relevant large-scale characteristics reported in this paper are based. In summary, as Re is increased in the simulations, vertical resolution is adjusted to be comparable to that of an equivalent DNS, and horizontal resolution and spectral filter are adjusted to allow for a broader dynamic range of the turbulence over the resolved scales. Consequently, one has confidence in reliably capturing, as a function of Re, the transition into the strongly stratified regime and the subsequent evolution of the large scales of the turbulence therein.

APPENDIX B: TIME DEPENDENCE OF TURBULENCE CHARACTERISTICS

In the investigation of the wake turbulence, it is of interest to understand how various turbulent diagnostics, such as length scales and turbulent kinetic energy, evolve with time. In this Appendix we first review the theory of decaying homogeneous stratified turbulence and then perform the necessary adaptations in the context of stratified wakes. It is important to note that the end results of the analysis are used as only a reference when interpreting the numerical results presented in Sec. V concerning stratified wakes; these results are by no means to be interpreted as generic results which are universal across all stratified flow configurations.

The theory for decaying homogeneous stratified turbulence [21,28,44,50] typically involves the following assumptions.

(i) Taylor's estimate for dissipation, i.e., Eq. (5), is valid, which leads to

$$\ell_h \sim \frac{\mathcal{U}^3}{\varepsilon}. \tag{B1}$$

While this relation is largely acceptable as a scaling argument, caution should be exercised when Taylor's estimate is used as an equality, i.e., $\varepsilon = A_k \mathcal{U}^3/\ell_h$, for stratified flows. Recent investigations [33,37] have revealed that the dimensionless number A_k may in fact vary as a function of time (e.g., Fig. 8 of Ref. [33] and Fig. 12 of Ref. [37]) when homogeneous turbulence decays from an initially energetic state.

(ii) Viscous dissipation dominates the turbulent kinetic energy (which is dominated by horizontal velocity $\mathcal{U}$) budget, i.e.,

$$\frac{1}{2}\frac{d\mathcal{U}^2}{dt} \sim -\varepsilon. \tag{B2}$$

(iii) The time dependence of turbulent quantities, such as $\mathcal{U}$, ℓ_h, and ε, can be expressed in terms of power laws, e.g.,

$$\mathcal{U} \propto t^{-n}, \tag{B3}$$

where n is a positive (as the turbulence is decaying) constant which needs to be determined. Squaring Eq. (B3) and substituting into Eq. (B2), one obtains

$$\varepsilon \propto t^{-2n-1}. \tag{B4}$$

Combining Eqs. (B1), (B3), and (B4), we obtain the time dependence of ℓ_h,

$$\ell_h \propto t^{-n+1}. \tag{B5}$$

While the value of n is still yet to be determined, one can already predict the time dependence of Fr_h following Eqs. (B3) and (B5):

$$\mathrm{Fr}_h \equiv \frac{\mathcal{U}}{N\ell_h} \propto t^{-1}. \tag{B6}$$

Such a scaling for Fr_h is a direct consequence of Taylor's estimate, i.e., Eq. (B1), and the assumption that viscous dissipation dominates the energy budget, i.e., Eq. (B2).

Further scaling predictions would require additional assumptions about the dynamics of turbulence. In order to proceed with making predictions for the time evolution of various quantities for wakes, we are motivated by the directly computed results shown in Fig. 10(a) to set the horizontal turbulent Reynolds number $\mathrm{Re}_h \equiv \mathcal{U}\ell_h/\nu$ to be a constant with time, i.e., $\mathcal{U}\ell_h \propto t^0$. It is then straightforward to deduce from Eqs. (B3)–(B5) that $n = 0.5$, and thus

$$\mathcal{U} \propto t^{-0.5}, \quad \ell_h \propto t^{0.5} \tag{B7}$$

under our stated assumptions. As shown in Sec. V, these scalings agree reasonably well with numerical data for a subset of the wakes simulated.

At this juncture, it is worth reiterating that the power laws of Eq. (B7) are founded on requiring (i) Taylor's estimate to hold, (ii) the viscous dissipation to be the dominant mechanism in the turbulent kinetic energy budget, and (iii) the horizontal turbulent Reynolds number Re_h to be constant in time (which itself is based on our observation). As such, these three requirements on which the predictions of Eq. (B7) rely do not necessarily coincide with the set of assumptions defining the strongly stratified regime, i.e., Eqs. (3), (4), and (6). Therefore, it is not expected that the validity of Eq. (B7) would be limited to the strongly stratified regime or that any flow in the strongly stratified regime would automatically follow Eq. (B7).

In the context of the evolution of a stratified wake past the initially active turbulent regime, the second requirement discussed previously, i.e., Eq. (B2), is most likely to hold in late wakes where shear production and internal wave radiation are expected to be weak. Recent studies [15,19],

however, have shown that both shear production and internal wave radiation could be comparable in magnitude to the viscous dissipation as the wake turbulence undergoes or completes the adjustment to buoyancy. For example, internal wave radiation has been independently found to be a leading-order term in the energy budget in the R400F4 case during the interval $10 \lesssim Nt \lesssim 40$ [17]. These additional considerations are addressed whenever relevant in the main text.

APPENDIX C: ESTIMATION OF STRATIFIED TURBULENCE CHARACTERISTICS

The stratified wake is a flow configuration that is geometrically distinct from triply periodic, box-filling turbulence in the sense that wake turbulence is localized in both y and z directions. Nevertheless, various diagnostics of stratified turbulence are computed for the wake under the assumption that the turbulent wake core may be approximated as homogeneous over a sufficiently large window in the wake cross section. Care should be taken in regard to the implications of such as assumption for the averaging procedures and vertical Fourier transforms used to compute spectra, both of which are essential for the estimation of the diagnostics of interest. This Appendix provides further details on the calculation of turbulent diagnostics from the spectra.

A first step towards computing the diagnostics of interest is to define the wake's turbulent core region (whose width and height may vary with time) over which turbulence statistics are first sampled locally and then averaged. We first apply the Reynolds decomposition to the velocity field, e.g., the streamwise velocity u can be decomposed into the mean and the fluctuating components

$$u(x, y, z, t) = \langle u \rangle_x(y, z, t) + u'(x, y, z, t), \tag{C1}$$

where $\langle \cdot \rangle_x$ denotes an average in the statistically homogeneous x direction. The $\langle u \rangle_x(y, z)$ profile for a given time becomes immediately useful for defining the dimensions of the wake core. Specifically, one assumes a self-similar two-dimensional Gaussian profile for $\langle u \rangle_x(y, z)$ as commonly used in experimental (e.g., [5]) and numerical (e.g., [10]) studies of stratified wakes, i.e.,

$$\langle u \rangle_x(y, z, t) = U_0(t) \exp\left[-\frac{1}{2}\left(\frac{y}{L_H(t)} \right)^2 - \frac{1}{2}\left(\frac{z}{L_V(t)} \right)^2 \right] \tag{C2}$$

for a wake centered at $(y, z) = (0, 0)$. For each snapshot of a simulation, a nonlinear least-squares fit is applied to the $\langle u \rangle_x(y, z)$ profile to determine the mean centerline velocity U_0 and the mean (half) wake width L_H and height L_V (for more details on their time evolution see Fig. 7.12 of Ref. [20]). The turbulence statistics reported in the main text are averaged over a volume encompassed by an elliptic cylinder, as defined by

$$\frac{y^2}{(2L_H)^2} + \frac{z^2}{(2L_V)^2} \leqslant 1, \tag{C3}$$

a region which is regarded as the turbulent wake core. This relatively simplistic definition of the wake core is adopted in this study for the ease of implementation, and we refer readers to Ref. [19] (whose focus was on the dynamics at the turbulent-nonturbulent interface) for a more sophisticated criterion for separating the turbulent and nonturbulent regions by thresholding local potential enstrophy values.

Making the assumption of homogeneity in a sufficiently large subarea of the cross section of the wake core, we employ turbulence spectra as a platform which drives estimates of turbulence length scales. In this paper the horizontal and vertical turbulence length scales ℓ_h and ℓ_v are estimated through the wake-averaged turbulence spectra, such as those shown in Fig. 14. Earlier analysis of the stratified wake data considered in this study [20,67] relied on alternative approaches which produced significant noise in the time series of these length scales, Instead, motivated by the approach used to analyze stratified homogeneous turbulence data [43], the horizontal turbulence length scale ℓ_h is

estimated via a weight-averaged inverse wave number, i.e.,

$$\ell_h \equiv \int_{k_{x,\min}}^{k_{x,\mathrm{Nyq}}} 2\pi k_x^{-1} E_u(k_x) dk_x \Big/ \int_{k_{x,\min}}^{k_{x,\mathrm{Nyq}}} E_u(k_x) dk_x, \tag{C4}$$

where $E_u(k_x)$ is the one-dimensional longitudinal spectrum of u velocity, which is spatially averaged over the wake core as defined by Eq. (C3); $k_{x,\min}$ is the minimum wave number $2\pi/L_x$; and $k_{x,\mathrm{Nyq}}$ is the Nyquist frequency given the available degrees of freedom in x. By not including $k_x = 0$, mean streamwise velocity effects are effectively ignored. Length scales so computed compare closely with those determined by the zero crossing of longitudinal autocorrelation functions [33], although the latter length scale estimate still exhibits some spurious fluctuations in time for the wake data and is thus not examined in detail.

Vertical spectra are also sampled for locations within the wake core, i.e., Eq. (C3). One-dimensional vertical profiles of the fluctuation component u' [as defined in Eq. (C1)] of the streamwise velocity are obtained for (x, y) locations with $y \in [-2L_H, 2L_H]$ and $x \in [0, L_x]$. They are then interpolated (using cubic splines) onto a uniform grid spanning the vertical window of $z \in [-2L_V, 2L_V]$, i.e., inside the wake core. Such an interval in z is chosen so that at the end points of the window, i.e., $z = \pm 2L_V$, the signal u' is sufficiently small such that the nonperiodicity introduced by the discontinuity of u' at the end points has a minimal impact on the spectra when periodicity is imposed by a Fourier transform. The vertical profiles of u' within the subwindow are Fourier transformed and then averaged for all (x, y) locations sampled to obtain the wake-averaged spectrum, i.e., $E_{u'}(k_z)$. Such a spectrum is then used to obtain an estimate for the vertical turbulence length scale ℓ_v, i.e.,

$$\ell_v \equiv \int_{k_{z,\min}}^{k_{z,\mathrm{Nyq}}} 2\pi k_z^{-1} E_{u'}(k_z) dk_z \Big/ \int_{k_{z,\min}}^{k_{z,\mathrm{Nyq}}} E_{u'}(k_z) dk_z, \tag{C5}$$

where $k_{z,\min}$ is the minimum wave number $2\pi/4L_V$ and $k_{z,\mathrm{Nyq}}$ is the Nyquist frequency. It is perhaps worth noting that the above definition of ℓ_v is based on the vertical spectrum of the fluctuation velocity u' as defined in Eq. (C1). Including the mean component $\langle u \rangle_x$, which is strongly sheared in the vertical direction z, would bias the estimate of ℓ_v in Eq. (C5) towards small wave numbers (larger scales) that are comparable to $k_{z,\min}$ rather than robustly describing the scale representative of the smaller-scale buoyancy-driven shear layers (see Fig. 5 for an example). Our use of the calculated vertical spectra is mainly to derive a characteristic integral length ℓ_v, and a detailed investigation of the vertical spectra (see, e.g., [68]) is outside the scope of this paper.

[1] G. R. Spedding, Wake signature detection, Annu. Rev. Fluid Mech. **46**, 273 (2014).

[2] M. Bonnier and O. Eiff, Experimental investigation of the collapse of a turbulent wake in a stably stratified fluid, Phys. Fluids **14**, 791 (2002).

[3] J. M. Chomaz, P. Bonneton, A. Butet, and E. J. Hopfinger, Vertical diffusion of the far wake of a sphere moving in a stratified fluid, Phys. Fluids **5**, 2799 (1993).

[4] J.-T. Lin and Y.-H. Pao, Wakes in stratified fluids, Annu. Rev. Fluid Mech. **11**, 317 (1979).

[5] G. R. Spedding, The evolution of initially turbulent bluff-body wakes at high internal Froude number, J. Fluid Mech. **337**, 283 (1997).

[6] G. R. Spedding, Vertical structure in stratified wakes with high initial Froude number, J. Fluid Mech. **454**, 71 (2002).

[7] G. R. Spedding, F. K. Browand, and A. M. Fincham, Turbulence, similarity scaling and vortex geometry in the wake of a towed sphere in a stably stratified fluids, J. Fluid Mech. **314**, 53 (1996).

[8] K. A. Brucker and S. Sarkar, A comparative study of self-propelled and towed wakes in a stratified fluid, J. Fluid Mech. **652**, 373 (2010).

[9] P. J. Diamessis, J. A. Domaradzki, and J. S. Hesthaven, A spectral multidomain penalty method model for the simulation of high Reynolds number localized incompressible stratified turbulence, J. Comput. Phys. **202**, 298 (2005).

[10] P. J. Diamessis, G. R. Spedding, and J. A. Domaradzki, Similarity scaling and vorticity structure in high-Reynolds-number stably stratified turbulent wakes, J. Fluid Mech. **671**, 52 (2011).
[11] D. G. Dommermuth, J. W. Rottman, G. E. Innis, and E. A. Novikov, Numerical simulation of the wake of a towed sphere in a weakly stratified fluid, J. Fluid Mech. **473**, 83 (2002).
[12] M. J. Gourlay, S. C. Arendt, D. C. Fritts, and J. Werne, Numerical modeling of initially turbulent wakes with net momentum, Phys. Fluids **13**, 3783 (2001).
[13] A. Pal, S. Sarkar, A. Posa, and E. Balaras, Direct numerical simulation of stratified flow past a sphere at a subcritical Reynolds number of 3700 and moderate Froude number, J. Fluid Mech. **826**, 5 (2017).
[14] A. Pal, M. B. de Stadler, and S. Sarkar, The spatial evolution of fluctuations in a self-propelled wake compared to a patch of turbulence, Phys. Fluids **25**, 095106 (2013).
[15] J. A. Redford, T. S. Lund, and G. N. Coleman, A numerical study of a weakly stratified turbulent wake, J. Fluid Mech. **776**, 568 (2015).
[16] A. M. Abdilghanie and P. J. Diamessis, The internal gravity wave field emitted by a stably stratified turbulent wake, J. Fluid Mech. **720**, 104 (2013).
[17] K. L. Rowe, P. J. Diamessis, and Q. Zhou, Internal gravity wave radiation from a stratified turbulent wake (unpublished).
[18] Q. Zhou and P. J. Diamessis, Surface manifestation of internal waves emitted by submerged localized stratified turbulence, J. Fluid Mech. **798**, 505 (2016).
[19] T. Watanabe, J. J. Riley, S. M. de Bruyn Kops, P. J. Diamessis, and Q. Zhou, Turbulent/non-turbulent interfaces in wakes in stably stratified fluids, J. Fluid Mech. **797**, R1 (2016).
[20] Q. Zhou, Far-field evolution of turbulence-emitted internal waves and Reynolds number effects on a localized stratified turbulent flow, Ph.D. thesis, Cornell University, 2015, https://hdl.handle.net/1813/41151.
[21] J. J. Riley, R. W. Metcalfe, and M. A. Weissman, Direct numerical simulations of homogeneous turbulence in density-stratified fluids, in *Proceedings of the La Jolla Institute Conference on Nonlinear Properties of Internal Waves, La Jolla, 1981*, edited by B. J. West, AIP Conf. Proc. No. 76 (American Institute of Physics, Woodbury, 1981), pp. 79–112.
[22] D. K. Lilly, Stratified turbulence and the mesoscale variability of the atmosphere, J. Atmos. Sci. **40**, 749 (1983).
[23] P. Billant and J.-M. Chomaz, Self-similarity of strongly stratified inviscid flows, Phys. Fluids **13**, 1645 (2001).
[24] G. Brethouwer, P. Billant, E. Lindborg, and J.-M. Chomaz, Scaling analysis and simulation of strongly stratified turbulent flows, J. Fluid Mech. **585**, 343 (2007).
[25] E. Lindborg, The energy cascade in a strongly stratified fluid, J. Fluid Mech. **550**, 207 (2006).
[26] J. J. Riley and S. M. de Bruyn Kops, Dynamics of turbulence strongly influenced by buoyancy, Phys. Fluids **15**, 2047 (2003).
[27] M. L. Waite and P. Bartello, Stratified turbulence dominated by vortical motion, J. Fluid Mech. **517**, 281 (2004).
[28] J. J. Riley and M.-P. Lelong, Fluid motions in the presence of strong stable stratification, Annu. Rev. Fluid Mech. **32**, 613 (2000).
[29] B. R. Sutherland, U. Achatz, C. P. Caulfield, and J. M. Klymak, Recent progress in modeling imbalance in the atmosphere and ocean, Phys. Rev. Fluids **4**, 010501 (2019).
[30] P. A. Davidson, *Turbulence in Rotating, Stratified and Electrically Conducting Fluids* (Cambridge University Press, Cambridge, 2013).
[31] G. I. Taylor, Statistical theory of turbulence, Proc. R. Soc. London Ser. A **151**, 421 (1935).
[32] G. N. Ivey, K. B. Winters, and J. R. Koseff, Density stratification, turbulence, but how much mixing? Annu. Rev. Fluid Mech. **40**, 169 (2008).
[33] A. Maffioli and P. A. Davidson, Dynamics of stratified turbulence decaying from a high buoyancy Reynolds number, J. Fluid Mech. **786**, 210 (2016).
[34] R. Godoy-Diana, J.-M. Chomaz, and P. Billant, Vertical length scale selection for pancake vortices in strongly stratified viscous fluids, J. Fluid Mech. **504**, 229 (2004).
[35] P. K. Kundu and I. M. Cohen, *Fluid Mechanics*, 4th ed. (Academic, New York, 2008).

[36] P. Augier and P. Billant, Onset of secondary instabilities on the zigzag instability in stratified fluids, J. Fluid Mech. **682**, 120 (2011).
[37] S. M. de Bruyn Kops and J. J. Riley, The effects of stable stratification on the decay of initially isotropic homogeneous turbulence, J. Fluid Mech. **860**, 787 (2019).
[38] P. Bartello and S. M. Tobias, Sensitivity of stratified turbulence to the buoyancy Reynolds number, J. Fluid Mech. **725**, 1 (2013).
[39] M.-P. Lelong and J. J. Riley, Internal wave-vortical mode interactions in strongly stratified flow, J. Fluid Mech. **232**, 1 (1991).
[40] C. J. Lang and M. L. Waite, Scale-dependent anisotropy in forced stratified turbulence, Phys. Rev. Fluids **4**, 044801 (2019).
[41] M. L. Waite, Stratified turbulence at the buoyancy scale, Phys. Fluids **23**, 066602 (2011).
[42] M. L. Waite, in *Modeling Atmospheric and Oceanic Flow*, edited by T. von Larcher and P. Williams (American Geophysical Union, Washington, DC, 2012), pp. 159–175.
[43] S. M. de Bruyn Kops (private communication).
[44] P. A. Davidson, On the decay of Saffman turbulence subject to rotation, stratification or an imposed magnetic field, J. Fluid Mech. **663**, 268 (2010).
[45] A. M. Fincham, T. Maxworthy, and G. R. Spedding, Energy dissipation and vortex structure in freely decaying, stratified grid turbulence, Dyn. Atmos. Oceans **23**, 155 (1996).
[46] F. S. Godeferd and C. Staquet, Statistical modeling and direct numerical simulations of decaying stably stratified turbulence. Part 2. Large-scale and small-scale anisotropy, J. Fluid Mech. **486**, 115 (2003).
[47] O. Praud, A. M. Fincham, and J. Sommeria, Decaying grid turbulence in a strongly stratified fluid, J. Fluid Mech. **522**, 1 (2005).
[48] S. M. Schaad and S. K. Venayagamoorthy, Direct numerical simulations of stably stratified decaying unforced turbulence, Comput. Fluids **158**, 2 (2017).
[49] C. Staquet and F. S. Godeferd, Statistical modeling and direct numerical simulations of decaying stably stratified turbulence. Part 1. Flow energetics, J. Fluid Mech. **360**, 295 (1998).
[50] J. J. Riley and E. Lindborg, Recent progress in stratified turbulence, in *Ten Chapters in Turbulence*, edited by P. A. Davidson, Y. Kaneda, and K. R. Sreenivasan (Cambridge University Press, Cambridge, 2012), pp. 269–317.
[51] P. Augier, P. Billant, and J.-M. Chomaz, Stratified turbulence forced with columnar dipoles: Numerical study, J. Fluid Mech. **769**, 403 (2015).
[52] G. R. Spedding, F. K. Browand, and A. M. Fincham, The long-time evolution of the initially turbulent wake of a sphere in a stable stratification, Dyn. Atmos. Oceans **23**, 171 (1996).
[53] P. Meunier, P. J. Diamessis, and G. R. Spedding, Self-preservation in stratified momentum wakes, Phys. Fluids **18**, 106601 (2006).
[54] M. L. Waite, The vortex instability pathway in stratified turbulence, J. Fluid Mech. **716**, 1 (2013).
[55] S. Basak and S. Sarkar, Dynamics of a stratified shear layer with horizontal shear, J. Fluid Mech. **568**, 19 (2006).
[56] P. Billant and J.-M. Chomaz, Theoretical analysis of the zigzag instability of a vertical columnar vortex pair in a strongly stratified fluid, J. Fluid Mech. **419**, 29 (2000).
[57] A. Deloncle, P. Billant, and J.-M. Chomaz, Nonlinear evolution of the zigzag instability in stratified fluids: A shortcut on the route to dissipation, J. Fluid Mech. **599**, 229 (2008).
[58] D. Lucas, C. P. Caulfield, and R. R. Kerswell, Layer formation in horizontally forced stratified turbulence: Connecting exact coherent structures to linear instabilities, J. Fluid Mech. **832**, 409 (2017).
[59] M. L. Waite and P. K. Smolarkiewicz, Instability and breakdown of a vertical vortex pair in a strongly stratified fluid, J. Fluid Mech. **606**, 239 (2008).
[60] J. R. Taylor and Q. Zhou, A multi-parameter criterion for layer formation in a stratified shear flow using sorted buoyancy coordinates, J. Fluid Mech. **823**, R5 (2017).
[61] Q. Zhou, J. R. Taylor, C. P. Caulfield, and P. F. Linden, Diapycnal mixing in layered stratified plane Couette flow quantified in a tracer-based coordinate, J. Fluid Mech. **823**, 198 (2017).
[62] S. B. Pope, *Turbulent Flows* (Cambridge University Press, Cambridge, 2000).

[63] S. B. Pope, Ten questions concerning the large-eddy simulation of turbulent flows, New J. Phys. **6**, 35 (2004).

[64] F. K. Chow and P. Moin, A further study of numerical errors in large-eddy simulations, J. Comput. Phys. **184**, 366 (2003).

[65] B. Vreman, B. Geurts, and H. Kuerten, Large-eddy simulation of the turbulent mixing layer, J. Fluid Mech. **339**, 357 (1997).

[66] P. J. Diamessis, Y.-C. Lin, and J. A. Domaradzki, Effective numerical viscosity in spectral multidomain penalty method-based simulations of localized turbulence, J. Comput. Phys. **227**, 8145 (2008).

[67] Q. Zhou and P. J. Diamessis, Reynolds number effects in stratified turbulent wakes, in *Proceedings of the VIIIth International Symposium on Stratified Flows, San Diego* (2016), https://escholarship.org/uc/item/1q3025d2.

[68] A. Maffioli, Vertical spectra of stratified turbulence at large horizontal scales, Phys. Rev. Fluids **2**, 104802 (2017).